ADVANCED MATERIALS
www.advmat.de

Applications of Ultrasound to the Synthesis of Nanostructured Materials

By *Jin Ho Bang* and *Kenneth S. Suslick**

Recent advances in nanostructured materials have been led by the development of new synthetic methods that provide control over size, morphology, and nano/microstructure. The utilization of high intensity ultrasound offers a facile, versatile synthetic tool for nanostructured materials that are often unavailable by conventional methods. The primary physical phenomena associated with ultrasound that are relevant to materials synthesis are cavitation and nebulization. Acoustic cavitation (the formation, growth, and implosive collapse of bubbles in a liquid) creates extreme conditions inside the collapsing bubble and serves as the origin of most sonochemical phenomena in liquids or liquid-solid slurries. Nebulization (the creation of mist from ultrasound passing through a liquid and impinging on a liquid-gas interface) is the basis for ultrasonic spray pyrolysis (USP) with subsequent reactions occurring in the heated droplets of the mist. In both cases, we have examples of phase-separated attoliter microreactors: for sonochemistry, it is a hot gas inside bubbles isolated from one another in a liquid, while for USP it is hot droplets isolated from one another in a gas. Cavitation-induced sonochemistry provides a unique interaction between energy and matter, with hot spots inside the bubbles of ~5000 K, pressures of ~1000 bar, heating and cooling rates of $>10^{10}$ K s^{-1}; these extraordinary conditions permit access to a range of chemical reaction space normally not accessible, which allows for the synthesis of a wide variety of unusual nanostructured materials. Complementary to cavitational chemistry, the microdroplet reactors created by USP facilitate the formation of a wide range of nanocomposites. In this review, we summarize the fundamental principles of both synthetic methods and recent development in the applications of ultrasound in nanostructured materials synthesis.

1. Introduction

Nanoscience and nanotechnology have grown at an enormous rate for the last three decades, and recent advances in nanostructured materials have opened up new opportunities for diverse applications in electronics, catalysis, energy, materials chemistry and even biology. Materials in the nanometer-size regime often exhibit properties distinct from their bulk counterparts, in part because clusters that small have electronic structures that have a high density of states, but not yet continuous bands. Nanostructured materials have been prepared by a variety of synthetic methods, including gas phase techniques (e.g., molten metal evaporation, flash vacuum thermal and laser pyrolysis decomposition of volatile organometallics), liquid phase methods (e.g., reduction of metal halides with various strong reductants, colloidal techniques with controlled nucleation), and mixed phase approaches (e.g., synthesis of conventional heterogeneous catalysts on oxide supports, metal atom vapor deposition into cryogenic liquids, explosive shock synthesis). One could claim that selecting an appropriate synthetic route ultimately determines the success or failure of nanostructured materials synthesis, because physical properties and applications of nanostructured materials are heavily dependent upon how they are prepared. The importance of choosing a proper synthetic route in designing nanostructured materials has been a driving force for the development of new methodologies for several decades. Indeed, this has led scientists' interest to the development of versatile and generalized synthetic methods readily adaptable for the preparation of a variety of nanostructured materials. Among a variety of approaches, the utilization of ultrasound for materials synthesis has been extensively examined over many years, and is now positioned as one of the most powerful tools in nanostructured materials synthesis. In this review, the two most successful ultrasound-assisted synthetic methods (sonochemistry and ultrasonic spray pyrolysis) will be discussed to provide a fundamental understanding of their basic principles and to demonstrate the powerful and unique aspects of ultrasound in nanostructured materials synthesis.

[*] Prof. K. S. Suslick, Dr. J. H. Bang
School of Chemical Sciences
University of Illinois at Urbana-Champaign
600 South Mathews Avenue, Urbana, Illinois 61801 (USA)
E-mail: ksuslick@illinois.edu

DOI: 10.1002/adma.200904093

2. Sonochemistry

2.1. Acoustic Cavitation

Chemistry deals with the interaction between energy and matter, and chemical reactions require some form of energy (e.g., heat,

© 2010 WILEY-VCH Verlag GmbH & Co. KGaA, Weinheim

REVIEW

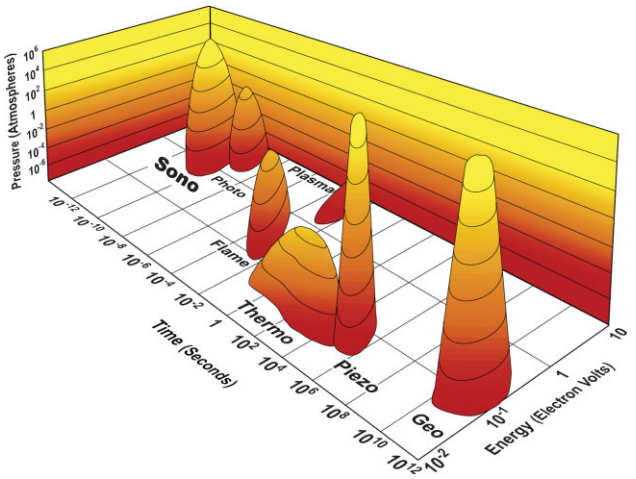

Figure 1. Islands of chemistry as a function of time, pressure, and energy. Adapted from [2] with permission. Copyright 1990, American Association for the Advancement of Science.

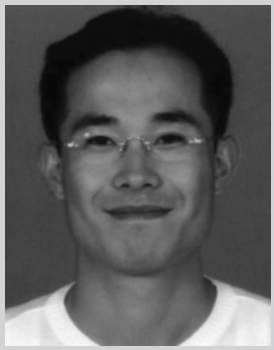

Jin Ho Bang received his B.S. and M.S. degrees from Seoul National University in 1999 and 2001, respectively. During his graduate studies in South Korea, he majored in electrochemistry under the supervision of Professor Hasuck Kim. After earning a M.S. degree, he moved to the University of Illinois at Urbana-Champaign in 2003 and received his Ph.D. degree in 2008. Under the guidance of Professor Kenneth S. Suslick, he had worked on the synthesis of nanostructured materials and their applications, including hydrogen evolution photocatalysts, fuel cells, and cellular imaging. Currently, he is working on quantum dot solar cells with Professor Prashant V. Kamat at the University of Notre Dame as a postdoctoral research associate.

Kenneth S. Suslick received his B.S. from the California Institute of Technology in 1974, his Ph.D. from Stanford University in 1978, and came to the University of Illinois at Urbana-Champaign immediately thereafter. Currently, he is the Marvin T. Schmidt Professor of Chemistry and also a Professor of Materials Science and Engineering and of the Beckman Institute for Advanced Science and Technology. He is a fellow of the MRS, AAAS, and the Acoustical Society of America (ASA). His two major research areas are the chemical and physical effects of ultrasound (which includes nanomaterials synthesis and sonoluminescence) and the bioinorganic and materials chemistry of metalloporphyrins, and now especially their applications for chemical sensing and artificial olfaction.

light, radiation, electric potential, etc.) to proceed.[1,2] Precise control over chemical reactions is a key to the success of nanostructured materials synthesis, but currently such control is limited to the manipulations of various reaction parameters including time, energy input, and pressure. These parameters, however, are adjustable only within a certain boundaries defined by the energy source employed in reactions. Each type of energy has its own realm of reaction conditions determined by its inherent reaction parameters, as depicted in Figure 1.[3] Compared to traditional energy sources, ultrasonic irradiation provides rather unusual reaction conditions (a short duration of extremely high temperatures and pressures in liquids) that cannot be realized by other methods.

Interestingly, such extraordinary conditions are not derived directly from ultrasound itself: acoustic wavelengths are *much* larger than molecular dimensions. Thus, no direct, molecular-level interaction between ultrasound and the chemical species takes place. Instead, acoustic cavitation (i.e., the formation, growth, and implosive collapse of bubbles in liquids), driven by high intensity ultrasound accounts for the chemical effects of ultrasound.[4] When liquids are irradiated with ultrasound, the alternating expansive and compressive acoustic waves creates bubbles (i.e., cavities) and makes the bubbles oscillate (Figure 2). The oscillating bubbles can accumulate ultrasonic energy effectively while growing to a certain size (typically tens of μm). Under the right conditions, a bubble can overgrow and subsequently collapse, releasing the concentrated energy stored in the bubble within a very short time (with a heating and cooling rate of $>10^{10}$ K s^{-1}). This cavitational implosion is very localized and transient with a temperature of ~5000 K and a pressure of ~1000 bar.[2]

These extreme conditions created during acoustic cavitation can give rise to light emission. This intriguing physical phenomenon, known as sonoluminescence, was first observed during the ultrasonic irradiation of water in 1934 by Frenzel and Schultes,[5] and afterward, has been systematically investigated by several research groups. Because of the transient nature of acoustic cavitation, sonoluminescence has been explored as a spectroscopic probe to investigate reaction conditions (e.g., temperature and pressure) during ultrasonic irradiation.[6–13]

A variety of sonochemical apparatuses are commercially available with several designs: ultrasonic cleaning baths, direct-immersion ultrasonic horns, and flow reactors are common examples. Cleaning baths have insufficient intensity for most applications, but are useful for liquid-solid reactions with easily passivated but reactive solids (e.g., Li, Mg). A typical laboratory-scale sonochemical apparatus (Figure 3a) consists of a high-intensity ultrasonic titanium horn driven by a piezoelectric transducer which is directly introduced into a thermostated glass reactor having gas inlets and outlets.[2] Cavitation occurs over a very wide range of frequencies, from tens of Hz to tens of MHz; above that frequency regime, the intrinsic viscosity of liquids

WILEY InterScience DISCOVER SOMETHING GREAT
© 2010 WILEY-VCH Verlag GmbH & Co. KGaA, Weinheim

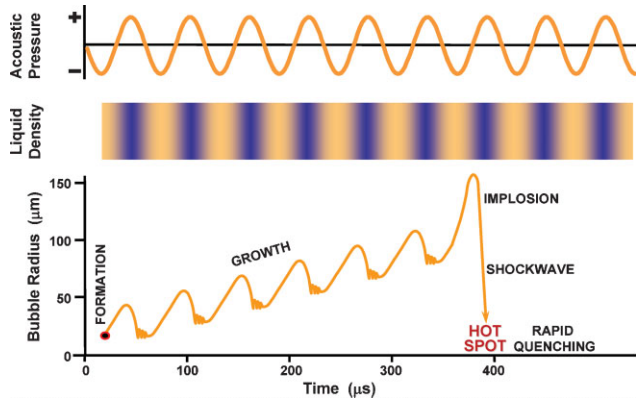

Figure 2. Schematic representation of transient acoustic cavitation. Adapted from [18] with permission. Copyright 1995, Materials Research Society.

prevents cavitation from occurring. Most high intensity ultrasonic horns operate at 20 or 40 kHz, most cleaning baths near 40 kHz, and there is specialized equipment available in the few hundred kHz to few MHz regime. In general, physical effects of ultrasound (e.g., emulsification and surface damage) are more dominant at lower frequencies, whereas cavitational heating of collapsing bubbles occurs over the full frequency range.

The chemical effects of ultrasound were explored for many years, nearly always in water.[14–17] Ultrasonic irradiation of aqueous liquids generates free radicals, and the formation of free radicals by sonolysis of water has been particularly well-studied. Primary sonolysis products in water are H· and OH· radicals.[17] These radicals can recombine to return to their original form or combine to produce H_2 and H_2O_2. They can also produce HO_2· by combination with O_2. These strong oxidants and reductants are utilized for various sonochemical reactions in aqueous solutions.

Major advancements in sonochemistry have been achieved by moving to less volatile organic liquids, so that the bubble contents are dominated by the intended reactants rather than the solvent vapor. Suslick and coworkers extensively explored the sonochemistry of metal carbonyl compounds (e.g., $Fe(CO)_5$, $Co(CO)_3NO$, $Mo(CO)_6$, and $W(CO)_6$) and utilized this non-conventional technique to produce unusual nanostructured inorganic materials.[2–4,18,19] They observed that volatile organometallic compounds can fully dissociate their carbonyl ligands inside a bubble during acoustic cavitation, and the resulting metal atoms agglomerate to form a variety of nanostructured materials. A powerful aspect of the sonochemical synthesis resides in its versatility; various forms of nanostructured metals, oxides, sulfides and carbides can be prepared simply by changing reaction conditions (Figure 3b).[2,4,18–20] For instance, sonochemical decomposition of $Fe(CO)_5$ in hexadecane yields amorphous iron metal powder.[21,22] In the presence of organic or polymeric stabilizers (e.g., oleic acid or polyvinylpyrrolidone), colloidal iron nanoparticles are obtained instead.[23] Adding a sulfur source into the precursor solution produces nanophase iron sulfide, and replacing argon gas with oxygen as the purging gas leads to the formation of nanoscale iron oxide. Further, when $Fe(CO)_5$ is irradiated with a solid support material (e.g., silica), nanometer-sized iron particles are deposited on the support.

2.2. Sonochemical Synthesis of Nanostructured Materials

2.2.1. Metals

Sonochemical syntheses of nanostructured noble metals (e.g., Au, Ag, Pt, and Pd) have been explored by a number of groups. Sonochemical reduction of noble metal salts has advantages over other traditional reduction methods (e.g., sodium borohydride, hydrogen, and alcohol): no chemical reducing agent is needed, the reaction rates are reasonably fast, and very small metal particles are produced.[24–29] As discussed earlier, sonolysis of water accounts for these sonochemical reductions; more specifically, sonochemically generated H· radicals are considered to act as reductants, as summarized below; often, organic additives (e.g., 2-propanol or surfactants) are added to produce a secondary radical species, which can significantly promote the reduction rate:

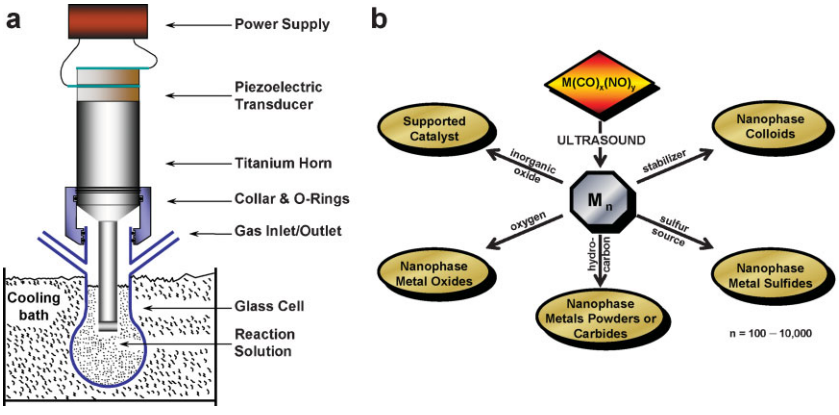

Figure 3. a) Typical high-intensity ultrasonic rig and b) sonochemical synthesis of various nanostructured inorganic materials. Reproduced with permission from [19]. Copyright 1999 Annual Reviews.

$$H_2O \rightarrow H\cdot + OH\cdot \quad (1)$$

$$H\cdot + H\cdot \rightarrow H_2 \quad (2)$$

$$H\cdot + OH\cdot \rightarrow H_2O \quad (3)$$

$$RH + OH\cdot \text{ (or } H\cdot) \rightarrow R\cdot + H_2O \text{ (or } H_2) \quad (4)$$

$$OH\cdot + OH\cdot \rightarrow H_2O_2 \quad (5)$$

$$\text{Au (III) (Ag(I), Pt (II), or Pd (II))} + H\cdot \text{ or } R\cdot \rightarrow \text{Au (0) (Ag(0), Pt (0), or Pd(0))} \quad (6)$$

$$nM(0) \rightarrow M_n \text{ (M = noble metal)} \quad (7)$$

© 2010 WILEY-VCH Verlag GmbH & Co. KGaA, Weinheim

Various metallic colloids have been prepared via the sonochemical route by many research groups.[24–30] Among them, Grieser and coworkers carried out a systematic study on sonochemical reduction to unveil the complex reduction mechanism and to understand the effect of each parameter (e.g., time, concentration, ultrasonic frequency, and different organic additives) on particle size and shape.[27,31–34] One of the interesting observations they reported is that particle size is inversely dependent upon alcohol concentration and alkyl chain length.[27] This is intimately related to the fact that alcohols adsorbed on the surface of metal nuclei can limit growth rate and also stabilize particles at a smaller size to prevent further growth. In addition, the rate of sonochemical reduction strongly relies on ultrasonic frequency, at least within the range of the specific experimental apparatus used in those studies, suggesting that frequency can play a role in controlling particle size.[31] The origin of the frequency effect, however, is not unambiguous and generally reflects upon the frequency dependent efficiency of the specific apparatus. Because sonochemical reactors are subject to standing waves, especially at higher frequencies, the volume where active cavitating bubbles occur and hence the number of cavitating bubbles is frequency and apparatus dependent. The effect of frequency is therefore difficult to assess independently of the apparatus itself.

Nanostructured metals were first prepared in non-aqueous solutions. Suslick and coworkers have developed a novel route to prepare nanostructured amorphous iron metal (Figure 4a) and colloidal iron nanoparticles (Figure 4b).[21–23] Highly volatile iron pentacarbonyl decomposes into iron atoms during sonication, and depending on the presence of an organic or polymeric stabilizer, either agglomerates of nanoparticles or colloidal nanoparticles are obtained. Stabilizers (e.g., oleic acid or polyvinyl-pyrrolidone) can trap the sonochemically decomposed iron nanoclusters before aggregation, resulting in colloidal nanoparticles. The amorphous iron metal powder has a high surface area of $\sim 150\,m^2\,g^{-1}$, owing to its porous and coral-like structure, and the sonochemically prepared colloidal iron nanoparticles show narrow size distributions centered at ~8 nm and are found to be superparamagnetic. The amorphous nature of sonochemically prepared iron results from the enormously fast cooling rates of hot spots during acoustic cavitation (i.e., solidification precedes crystallization).

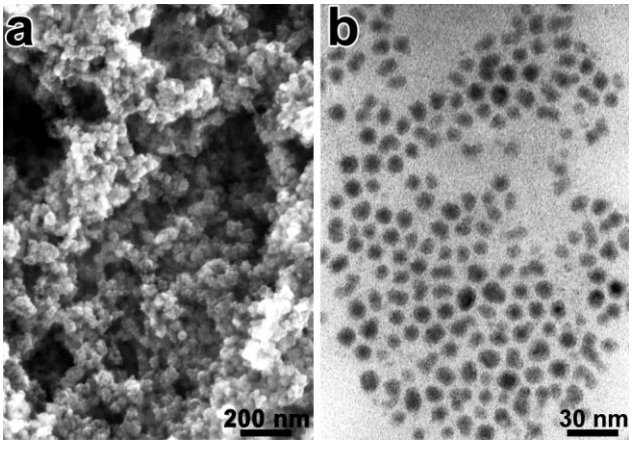

Figure 4. Sonochemically prepared a) amorphous iron (reproduced with permission from [37], Copyright 1996 American Chemical Society) and b) iron colloid (reproduced with permission from [23], Copyright 1996 American Chemical Society).

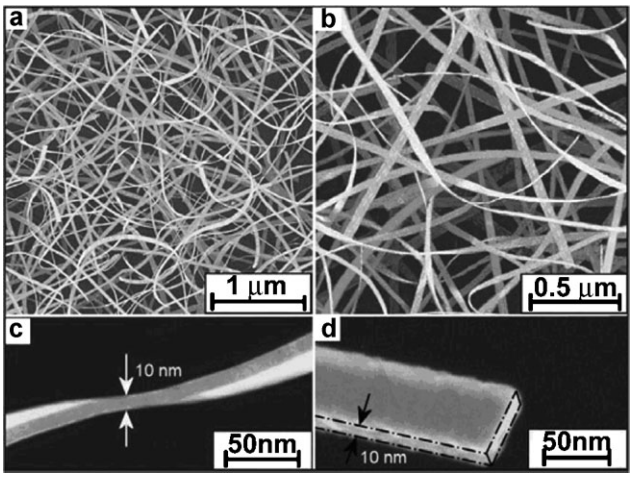

Figure 5. Sonochemically prepared gold nanobelts. Reproduced with permission from [24].

In general, sonochemical synthesis produces spherical metal nanoparticles, and thus the sonochemical process had been limited in preparing other metal nanostructures (e.g., nanorods, nanowires, etc.). Recently, Han and coworkers reported an intriguing result on shape control.[24] In their synthetic approach, ultrasonic irradiation of an aqueous $HAuCl_4$ solution containing α-D-glucose produces gold nanobelts having a width of 30–50 nm and a length of several micrometers (Figure 5). Mechanistic study revealed that ultrasonic irradiation dramatically enhances the Ostwald ripening process via acoustic cavitation induced turbulence (e.g., microstreaming and shock waves). Thus, with α-D-glucose as a structure-directing agent, nanobelts can be formed by merging gold nanoparticles produced at an early stage of sonication.

Another shape control method using ultrasound was reported by Liz-Marzán and coworkers.[35,36] They synthesized monodispersed gold nanodecahedra with high yield and noticeably increased reproducibility via ultrasound-induced reduction of $HAuCl_4$ on pre-synthesized gold seeds in *N,N*-dimethylformamide (DMF) solution. Surprisingly, thermal reduction without the use of ultrasound produces a lower yield of gold decahedra with increased polydispersity. A similar synthetic strategy was exploited by Zhu and colleagues in the synthesis of silver nanoplates.[37] In their synthesis, the ultrasound-assisted Ostwald ripening process leads to the growth of silver nanoplates from silver nanoparticles formed at an early stage of reaction.

A novel synthetic strategy termed "sonochemical-assisted metal displacement reduction" was introduced by Zeng and coworkers for the synthesis of gold and platinum nanoparticles.[38] In their synthetic route, Au or Pt atoms are generated by reduction of their precursors on the surface of Cu or Fe foils (i.e., metal displacement reduction) under ultrasonic irradiation, and

WILEY InterScience DISCOVER SOMETHING GREAT
© 2010 WILEY-VCH Verlag GmbH & Co. KGaA, Weinheim

the shock wave induced by ultrasonic irradiation dislodges the atoms from the foil surfaces. The dispersed atoms then nucleate and grow into colloidal nanoparticles. While ultrasound is not directly employed to reduce novel metal salts in this reaction (i.e., sonochemical reduction), it is an interesting demonstration of the use of the physical effects of ultrasound (i.e., the effect of microjets and shockwaves on a solid surface) in the preparation of nanoparticles.

In addition to monometallic nanoparticles, colloidal bimetallic nanoparticles have been prepared by sonochemical synthetic routes. Bimetallic nanoparticles have been of great interest because of their increased use in catalysis and optoelectronic applications. Suslick and coworkers were the first to demonstrate the exploitation of ultrasound to produce bimetallic nanoparticles.[39–42] In their synthesis, sonochemical decomposition of iron pentacarbonyl ($Fe(CO)_5$) and cobalt tricarbonylnitrosyl ($Co(CO)_3(NO)$) yields Fe–Co alloys, and the composition of Fe–Co alloys was simply tuned by changing stoichiometric ratios of the two precursors in the gas phase via their respective vapor pressures. Surprisingly, the alloys are highly active toward dehydrogenation of alkanes, while iron or cobalt alone are a poor catalyst for this reaction. Lukehart and coworkers also prepared metal alloy nanoparticles from the sonochemical decomposition of a single-source precursor.[43] They first synthesized $Pt_3Fe_3(CO)_{15}$, a polyheteronuclear cluster complex, by reacting $Fe(CO)_5$ and tris(norbornylene)-platinum(0). Ultrasonic irradiation of this precursor solution of this precursor in the presence of oleic acid and oleylamine produces FePt nanoparticles, which have a high coercivity at room temperature.

Later groups have reported various bimetallic nanoparticles, mostly in aqueous or alcohol solutions via sonochemical reduction. Mizukoshi and coworkers reported a sonochemical synthesis of core-shell structured gold/palladium nanoparticles in aqueous solutions.[44,45] They monitored the surface plasmon absorption band of the precursor solution during sonication and elucidated the formation of a core-shell structure; the nucleation of the gold core precedes the reduction of palladium ions, in part because of a difference in redox potentials ($AuCl_4^-$/Au: 1.002V; $PdCl_4^{2-}$/Pd: 0.620 V). Shchukin and coworkers also reported various nanostructures of gold–silver nanocomposites in the presence of a surfactant via a successive sonochemical reduction.[46] Recently, Grieser and coworkers have synthesized Pt–Ru bimetallic nanoparticles with different stabilizers via a sequential sonochemical reduction.[32] Casadonte, Korzeniewski and coworkers examined the electrocatalytic activity of sonochemically prepared Pt–Ru bimetallic nanoparticles toward methanol oxidation and revealed that the Pt–Ru nanoparticles display bulk alloy properties.[47]

Sonochemical synthesis of metal nanostructures has not been confined to noble metals and their alloys. Xia and coworkers have developed a sonochemical synthetic route for trigonal selenium nanowires.[48,49] Trigonal selenium nanowires are inherently anisotropic, which allows one-dimensional nanostructure formation without the use of templates or surfactants. They noticed that sonication drives the anisotropic growth significantly faster than conventional recrystallization (i.e., hours vs. days) through an accelerated Ostwald ripening process and successfully converted spherical amorphous phase Se particles to trigonal Se nanowires with ~100% yield.

2.2.2. Metal Oxides

A myriad of metal oxides have been prepared by sonochemical techniques. Gedanken and coworkers have reported various nanostructured metal oxide syntheses including TiO_2,[50] Fe_3O_4,[51] α-$Ni(OH)_2$,[52] $GaO(OH)$,[53] $In(OH)_3$,[54] and $BaFe_{12}O_{19}$.[55] In their syntheses, sonication of an aqueous metal salt solution is carried out under ambient conditions (usually in the presence of air) to prepare various forms of nanostructured metal oxides. For instance, nanometer-sized α-nickel hydroxide was prepared simply by sonicating an aqueous solution of nickel nitrate and urea.[52] It is believed that ultrasonic irradiation significantly enhances the hydrolysis rate, and shock waves can induce unusual morphological changes in metal oxides.

The advantages of the sonochemical approach over conventional methods in the synthesis of metal oxides, including more uniform size distribution, a higher surface area, faster reaction time, and improved phase purity, have been recognized by many research groups. Examples of successful sonochemical syntheses include TiO_2,[56] ZnO,[57–59] CeO_2,[60] MoO_3,[61] V_2O_5,[62] In_2O_3,[63] $ZnFe_2O_4$,[64] $PbWO_4$,[65,66] $BiPO_4$,[67] and $ZnAl_2O_4$.[68] Yu and coworkers revealed that sonochemically prepared titania nanoparticles are more photocatalytically active than commercial titania nanoparticles (e.g., Degussa P25).[56] Such enhancement was attributed to improved crystallinity of titania caused by a faster hydrolysis rate in the presence of ultrasound.

Sonochemical preparation of metal oxides has been further extended to the synthesis of mesoporous (i.e., pores with diameters between 2 and 50 nm) metal oxides. It has been demonstrated by several research groups that ultrasonic irradiation significantly shortens the sol-gel reaction time needed to assemble mesostructures to a few hours. Considering that the reaction times required in conventional methods are often several days, such a dramatic reduction in the reaction time can be of great benefit. Gedanken and colleagues reported the sonochemical preparation of mesoporous titania with wormhole-like framework structures.[69] They sonicated an ethanol/water solution containing titanium isopropoxide ($Ti(^iOPr)_4$) and structure-directing agents (e.g., decylamine, dodecylamine, or octadecylamine) under ambient conditions for 6 h. The shortened reaction time was attributed to an extremely high temperature at the interface between a collapsing bubble and the bulk solution, which was presumed to hasten the hydrolysis and condensation of the titanium precursor; more likely, simple improvements in mass transport are actually responsible. Yu et al. reported hierarchically porous titania spheres synthesized via a sonochemical method where an ethanol/water solution containing titanium isopropoxide was ultrasonically irradiated for 3 h in the presence of a block copolymer.[70] They observed an enhanced photocatalytic activity of the porous titania spheres. Their synthetic approach was further developed to prepare mesoporous titania having a bicrystalline (anatase and brookite) framework with and without the use of a block copolymer.[71] This sonochemical approach was extended to nanoporous (i.e., pores in nanometer range between 100 and 0.2 nm) ceria, ceria-zirconia oxide solid solution, and even perovskite-type nanoporous oxides (e.g., $SrTiO_3$).[72,73]

The utilization of ultrasound has been further developed for the alignment of nanostructured metal oxides. Recent exciting

© 2010 WILEY-VCH Verlag GmbH & Co. KGaA, Weinheim

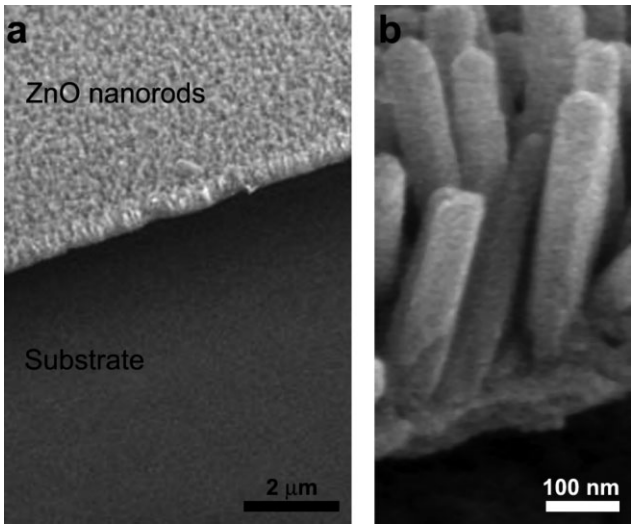

Figure 6. Tilt-view SEM images of vertically aligned ZnO rods produced using sonochemical-induced anisotropic growth of ZnO along the (0001). Reproduced with permission from [74].

work by Jeong and coworkers describes a robust and rapid synthetic route to prepare vertically aligned ZnO nanorods on a substrate,[74] as a useful demonstration of the employment of ultrasound in the direct growth of nanostructured materials on a substrate. In their work (Figure 6), ultrasonic irradiation rapidly induced anisotropic growth of ZnO along the (0001) direction on various substrates (e.g., Zn sheet, Si-wafer, glass, and polycarbonate). The alignment process is presumed to be due in part to the relative depletion of Zn^{+2} concentration at the base of the growing rods relative to the exposed tops of the rods. Compared to conventional approaches, such as a hydrothermal method, the growth rate of ZnO was increased more than tenfold, with an average growth rate of $\sim$500 nm h^{-1}. Because of the compatibility of this novel synthetic route with various substrates (especially Si-wafer), patterning ZnO nanorods can be easily achieved when this sonochemical synthesis is combined with traditional photolithography processes to localize the initial seeding. There are interesting potential applications to solar energy conversion for such oriented rod materials.

Ultrasonic treatment of metal oxide powders (i.e., liquid-powder slurries irradiated with high-intensity ultrasound) can bring unexpected improvements in physical properties. Ulman and coworkers sonochemically modified Fe_2O_3 with Mn(III) by sonicating a slurry of amorphous Fe_2O_3 nanoparticles and $Mn_2(CO)_{10}$ in decahydronaphthalene.[75] Mn(III)-doped γ-Fe_2O_3 obtained by subsequent calcination shows an unusual resistance to the phase transition from γ-Fe_2O_3 to more stable α-Fe_2O_3 during high temperature heat-treatment.

Suslick and coworkers significantly enhanced the superconducting properties of $Bi_2Sr_2CaCu_2O_{8+x}$ simply by applying high-intensity ultrasound to slurries of $Bi_2Sr_2CaCu_2O_{8+x}$ powder in decane.[76] Ultrasound-induced interparticle collisions led to a considerable enhancement of intergrain coupling, which governs the critical magnetic field (J_c) that limits the fields that can be generated using $Bi_2Sr_2CaCu_2O_{8+x}$ superconductor.

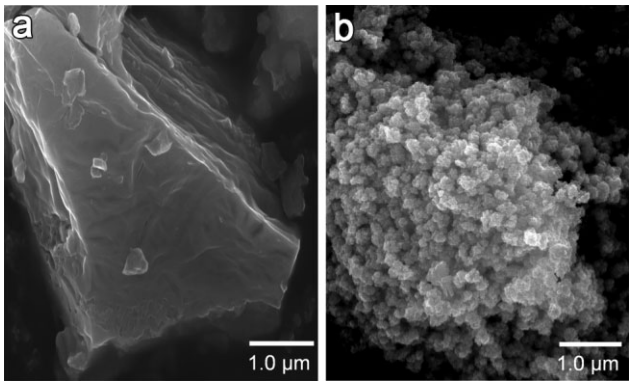

Figure 7. SEM images of a) conventionally and b) sonochemically prepared MoS_2. Reproduced with permission from [80]. Copyright 1998, American Chemical Society.

2.2.3. Metal Chalcogenides and Carbides

Various metal chalcogenides (e.g., CdS,[77,78] ZnS, PbS,[79] MoS_2,[80,81] Bi_2S_3,[82] CdSe,[77] ZnSe,[83] PbSe,[84] Bi_2Se_3,[85] β-CuSe,[86] Cu_3Se_2,[86] Cu_7Te_4,[87] Cu_4Te_3,[87] GaSb,[88] $AgBiS_2$[89], etc) have been prepared by sonochemical synthesis. A typical synthesis of these materials involves the ultrasonic irradiation of an aqueous solution of a metal salt and a chalcogen source (e.g., thiourea for sulfur or selenourea for Se): in situ generated H_2S or H_2Se by sonication reacts with metal salts to produce metal chalcogenide nanoparticles. Using a structure-directing agent, a variety of nanostructures (e.g., nanorods, nanowires, or nanocubes) have been prepared.[78,79,82,84,85]

The first sonochemical approach to metal chalcogenide synthesis, pioneered by Suslick and colleagues, was the sonication of organometallic precursors in the presence of a chalcogen source. Nanostructured MoS_2 was synthesized by irradiating a slurry of molybdenum hexacarbonyl ($Mo(CO)_6$) and sulfur in 1,2,3,5-tetramethylbenzene (isodurene) with high-intensity ultrasound.[80] A conventional method produces powder having the plate-like morphology typically seen in layered materials (Figure 7a). The sonochemically prepared MoS_2, however, exhibits an unusual morphology: a porous agglomeration of spherical particle clusters having an average size of 15 nm (Figure 7b). Transmission electron microscopy (TEM) examination reveals that both MoS_2 materials have the same interlayer spacing of 0.62 ± 0.01 nm in spite of the remarkable difference in morphology. Because of their nanoparticle nature, the sonochemically prepared MoS_2 has a higher surface area with much higher numbers of edges and defects on the surface than the conventionally obtained counterpart; in other words, the layers in nanoparticles must bend, break, or otherwise distort to fit to the radius of curvature of the outer surface.

MoS_2 has been heavily exploited as a hydrodesulfurization catalyst in the petroleum industry to remove sulfur from crude oil. It has been well-known that the hydrodesulfurization catalytic sites of MoS_2 are localized at the edges and not on the flat basal planes.[90] Suslick and coworkers compared the sonochemically prepared MoS_2 to conventional MoS_2 and commercial ReS_2 and RuS_2 catalysts.[80] While the ReS_2 and RuS_2 catalysts are innately more active than MoS_2,[91,92] their use has been severely limited

WILEY InterScience DISCOVER SOMETHING GREAT
© 2010 WILEY-VCH Verlag GmbH & Co. KGaA, Weinheim

because of their extremely high price. The sonochemically prepared MoS_2 is superior to conventional MoS_2 for the hydrodesulfurization of thiophene because of its nanostructure (which dramatically increases active edge surface area), and furthermore the catalytic activity of nanostructured MoS_2 is even comparable to that of RuS_2.

Sonochemical methods have also proved useful synthetic tools for the production of hollow metal chalcogenide nanostructures. Hollow inorganic spheres have attracted attention because of their potential utilization in diverse applications (e.g., catalysis, photonic materials, and even drug delivery). Typical synthetic routes involve the use of sacrificial template materials such as preformed colloids of silica or polymer, which makes the synthetic process complicated and inefficient in terms of time and cost. Sonochemical synthesis, however, provides a facile and rapid synthetic route to prepare hollow inorganic spheres often without the use of templates.

Zhu and coworkers reported sonochemical preparation of hollow assemblies of CdSe via an in situ template route.[93] In their sonochemical reaction, it was observed that amorphous $Cd(OH)_2$, an intermediate produced at an early state of the reaction, allows CdSe formation only on the surface, providing a hollow interior after dissolution of the remaining core of unreacted $Cd(OH)_2$. Vrinat and colleagues have synthesized hollow MoS_2 spheres by irradiating an aqueous solution of ammonium heptamolybdate ($(NH_3)_6Mo_7O_{24} \cdot 4H_2O$) with high-intensity ultrasound.[81] The formation of hollow microspheres is attributed to decomposition of ammonium heptamolybdate at the gas-liquid interface, which might permit cavitation bubbles to play a role as a hollow template; we view this as an interesting but unlikely speculation. Very recently, an ultrasound-assisted substitution reaction was introduced as a simple and fast chemical conversion method to prepare hollow structures. Zhu and coworkers sonicated ZnO nanospheres in the presence of either a sulfur or selenium source and were able to convert ZnO directly to hollow ZnS or ZnSe spheres.[94] In this method, in-situ generated S^{2-} or Se^{2-} is adsorbed onto the ZnO surface, providing initial nucleation sites for the surface growth of ZnS or ZnSe nanoparticles. The adsorbed S^{2-} or Se^{2-} can further diffuse into the inner part of solid ZnO because ZnO, composed of numerous nanocrystals, allows the chalcogen ions to penetrate with relative ease. The conversion of ZnO to hollow ZnS or ZnSe spheres is assumed to be related to the quick release of intermediate H_2S or N_2 gas or Oswald ripening. Another advantage of this synthetic route, along with its simplicity, is that various other nanostructures (e.g., simple solid and core/shell structures) can be easily obtained by slightly changing reaction conditions. With the assistance of a soft template (e.g., surfactants or even bacteria), the sonochemical method also produced hollow nanostructures of various metal sulfides.[95,96]

Sonochemical synthesis is found to be superior to traditional methods even in the production of high-quality semiconductor nanoparticles (i.e., quantum dots). In their recent report, Young and coworkers highlighted several advantages of a sonochemical procedure over thermal synthesis: better control over growth rate of nanocrystals via ultrasonic intensity and significantly lower reaction temperatures.[97] CdSe/ZnS core/shell quantum dots prepared by a two-step sonochemical process exhibit high photoluminescence, with quantum efficiencies of 50–60% and a narrow size distribution of ~10%. This facile synthetic route provides an alternative way for the large-scale synthesis of highly luminescent semiconductor nanoparticles.

Sonochemical synthesis also provides advantages in the synthesis of refractory metal carbides. Metal carbides (e.g., molybdenum and tungsten carbides) are, in general, prepared by reacting a metal and carbon at an extremely high temperature, and carbides themselves are inherently refractory. For these reasons, the preparation of nanostructured metal carbides with a large surface area and a high porosity has remained a substantial challenge for materials scientists. Suslick and coworkers have developed a facile sonochemical route to prepare nanostructured molybdenum and tungsten carbides (Mo_2C and W_2C, respectively).[98,99] In their synthesis, amorphous oxycarbides were first obtained by sonochemical decomposition of molybdenum hexacarbonyl or tungsten hexacarbonyl in hexadecane. The oxygen was then eliminated by heat-treatment under a 1:1 CH_4/H_2 mixture gas. This alternative route not only permits a low-temperature synthesis, but also enables the production of unprecedented nanostructures of carbides. Electron microscopy revealed that the obtained products are a porous aggregate of nanometer-sized particles (Figure 8a), and the surface areas of Mo_2C and W_2C were found to be 130 and 60 $m^2\,g^{-1}$, respectively.

Mo_2C and W_2C have been explored for heterogeneous catalysis (e.g., dehydrogenation and hydrodehalogenation), because their

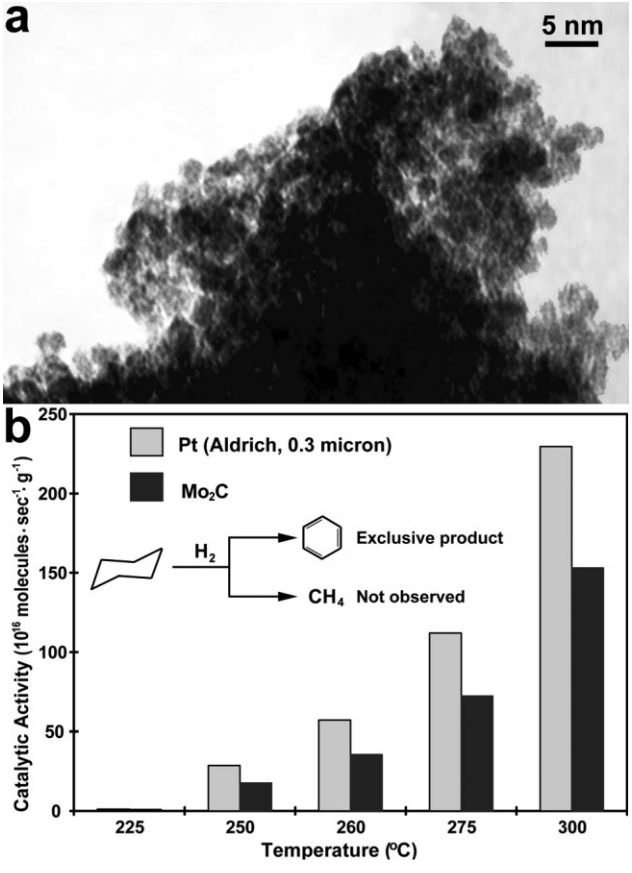

Figure 8. a) TEM image and b) catalytic activity for dehydrogenation of cyclohexane of sonochemically prepared Mo_2C. Reproduced with permission from [98]. Copyright 1996 American Chemical Society.

© 2010 WILEY-VCH Verlag GmbH & Co. KGaA, Weinheim

catalytic activities are comparable to those of platinum group metals. For instance, sonochemically produced Mo_2C was proven to be an excellent dehydrogenation catalyst, with activity and selectivity comparable to those of Pt metal (Figure 8b).[98] In addition, nanostructured molybdenum and tungsten carbides prepared by the sonochemical route show superior activity, selectivity, and stability for hydrodehalogenation of halogenated organic pollutants.[99]

2.2.4. Nanostructured Materials via Sonochemical Deposition

The physical effects of ultrasound (e.g., ultrasound-induced shock waves and microjets at the liquid–solid interface) are primarily responsible for unusual sonochemical effects such as generation of surface damage, high-speed interparticle collisions, and fragmentation of friable solids.[19] The impact of shock waves and microjets on solid particles suspended in liquids was demonstrated in the early works of the Suslick research group.[100–103] For instance, high-intensity ultrasound drives metal particles having a low-melting point (e.g., Zn and Sn) together at sufficiently high speeds to induce effective melting at the point of impact (Figure 9).[103,104]

The physical effects of ultrasound have often been utilized to deposit nanoparticles onto the surface of substrates. Gedanken and coworkers reported sonochemical deposition of in-situ generated noble metal nanoparticles on various substrates (e.g., silica, carbon, or polymer).[105–107] This sonochemical process significantly reduces the reaction time, achieving uniform coating of nanoparticles on substrates. Also, noble metal nanoparticles can be easily anchored on various substrates without tailoring surface properties (e.g., attaching thiols to the surface of a substrate) via this procedure.

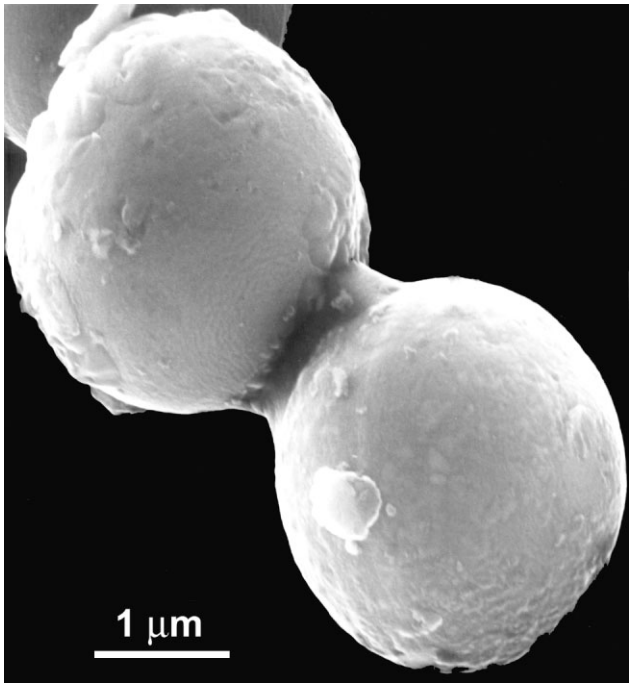

Figure 9. SEM image of a neck formed by interparticle collisions of Zn metal under ultrasonic irradiation. Reproduced with permission from [103]. Copyright 1990, American Association for the Advancement of Science.

In addition to noble metal deposition, a sonochemical route for coating metal oxide nanoparticles with silica or metal sulfides (e.g., CdS) has been demonstrated. A recent report by Nikitenko et al. describes sonochemical coating of silica over Fe_3O_4 nanoparticles.[108] In this work, ultrasonic irradiation significantly promotes the homogeneity of the hydrolysis of tetraethyl orthosilicate (TEOS) and prevents agglomeration of silica sols by improving the mass transport of silica sols to Fe_3O_4 nanoparticle surfaces, which results in homogeneously coated core–shell nanoparticles. Not only is the sol-gel reaction time significantly reduced, but also the thickness of silica coating over Fe_3O_4 nanoparticles can be easily manipulated by sonication time in this synthetic route. Ulman and coworkers have also reported sonochemical coating of silane over TiO_2 and γ-Fe_2O_3 nanoparticles.[109,110] Very recently, Chen and coworkers synthesized silica coating over indium tin oxide (ITO) nanoparticles via a sonochemical route.[111] Sonochemical deposition of metal sulfides over metal oxides provides an alternative way to produce hetero-structured core/shell composites. Gao and coworkers sonochemically synthesized core/shell hetero-structures of SnO_2/CdS and ZnO/CdS.[112,113] Ultrasonic irradiation also enhances polymer coatings on substrates. Atobe and colleagues have demonstrated that ultrasonically-induced turbulence lead to a uniform coating of polypyrrole on carbon fibers.[114]

Combining the physical and chemical effects of ultrasound, Suslick and Dantsin successfully prepared a bifunctional "eggshell catalyst", where the outer surface of ZSM-5 is decorated with nanometer-sized Mo_2C catalyst particles.[115] In the preparation of Mo_2C/ZSM-5 catalyst, a slurry of molybdenum hexacarbonyl and H-ZSM-5 zeolite in hexadecane was irradiated with high intensity ultrasound under an Ar flow. This facile sonochemical route produces uniformly dispersed Mo_2C nanoparticles of ~2 nm in diameter on the outer surface of ZSM-5, greatly improving upon the poor dispersion of nanoparticles formed in supported catalysts obtained by conventional methods (e.g., incipient wetness or ion exchange). While Mo_2C alone does not catalyze methane aromatization, the sonochemically produced bifunctional eggshell catalyst was found to be extremely active for this reaction.

Ultrasonic irradiation facilitates the formation of graphite intercalation compounds with unusual efficiency. Casadonte and coworkers have developed a facile sonochemical synthesis of KC_8, a powerful reducing agent widely used in organic reactions.[116] While a typical synthesis of KC_8 requires 1–2 days, the newly devised sonochemical synthesis is completed in less than 5 min. In this reaction, simple sonication of potassium and graphite in toluene for several minutes produces golden-bronze, metallic colored KC_8. Another example of the use of ultrasound in a graphite intercalation reaction was reported by Walter and coworkers,[117] who synthesized Pt nanoparticle-intercalated graphite via a sonochemical method.

Sonochemical deposition of inorganic nanoparticles on solid substrates (e.g., silica or carbon nanotubes) has been utilized to produce hollow nanostructures. Suslick and Dhas devised sonochemical syntheses of hollow MoS_2 and MoO_3 spheres.[118] Ultrasonic irradiation of an isodurene slurry of molybdenum hexacarbonyl, sulfur, and silica nanospheres under an Ar flow yields a MoS_2/SiO_2 composite. A similar procedure performed in the presence of air and the absence of sulfur produces a MoO_3/SiO_2 composite. Subsequent HF treatment leached out the silica spheres, resulting in hollow spheres of MoS_2 (Figure 10a and b)

WILEY InterScience DISCOVER SOMETHING GREAT
© 2010 WILEY-VCH Verlag GmbH & Co. KGaA, Weinheim

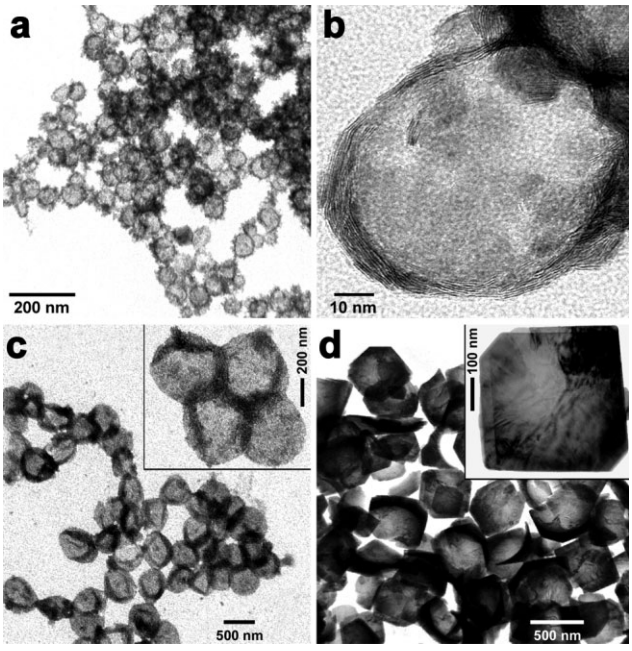

Figure 10. TEM images of sonochemically prepared hollow MoS_2 nanospheres (a and b) and hollow MoO_3 (c) after leaching of the silica template but before thermal annealing and after thermal annealing and formation of hollow single crystals (d). Reproduced with permission from [118]. Copyright 2005, American Chemical Society.

and MoO_3 (Figure 10c). Because of a significantly increased number of edge defects and improved accessibility to both inner and outer surfaces in hollow MoS_2 nanospheres, the catalytic activity of hollow MoS_2 toward hydrodesulfurization of thiophene is superior to that of sonochemically prepared nanostructured and conventional micron-sized counterparts. Interestingly, upon heat-treatment, the hollow MoO_3 spheres undergo an unusual phase transformation to truncated cubic hollow crystals, yielding the first ever hollow single crystals (Figure 10d).

Very recently, Suslick and Bang reported sonochemical synthesis of nanometer-sized hollow hematite (Figure 11).[119] In this novel synthesis, carbon nanoparticles were exploited as a spontaneously removable template. The mechanism of the hollow hematite formation utilizes in situ combustion of the carbon nanoparticles: amorphous iron nanoparticles produced from sonochemical decomposition of $Fe(CO)_5$ form shells around the pre-existing carbon nanoparticles. Upon exposure to oxygen, the heat released from rapid oxidation of the high surface area iron shells ignites the internal carbon particles. The combustion of the nanometer-sized carbon particles generates enough heat to crystallize the iron oxide shells, converting them to α-Fe_2O_3 with remnant hollow cores.

A related effort by Yang and coworkers recently reported the synthesis of porous Co_3O_4 nanotubes via a sonochemical route.[120] Carbon nanotubes (CNTs) were exploited as a sacrificial template in this synthesis, and a sonochemically prepared CoO_x/CNTs composite was calcined under air to burn away the carbon nanotubes and to crystallize the amorphous CoO_x into Co_3O_4. The porous Co_3O_4 nanotubes were found to be an excellent electrode material in lithium batteries.

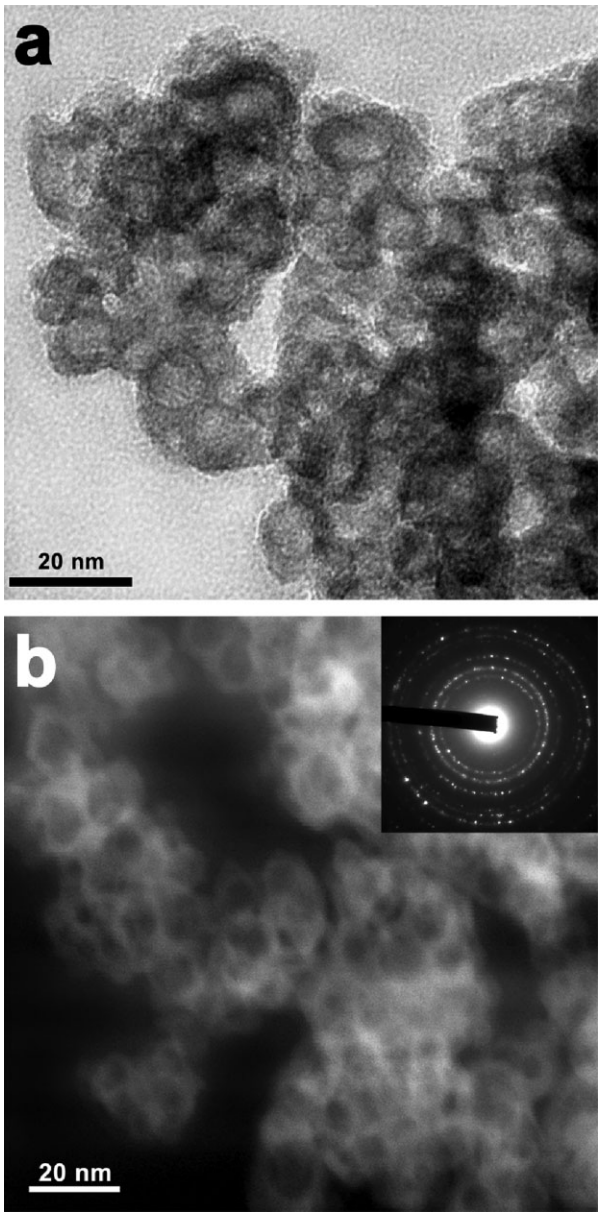

Figure 11. a) Bright-field TEM image and b) dark-field TEM image (inset: selected area electron diffraction pattern) of nanometer-sized hollow hematite. Reproduced with permission from [119]. Copyright 2007, American Chemical Society.

Loh and coworkers further extended the sonochemical deposition technique to prepare hollow FePt spheres.[121] Sonochemically produced FePt particles were deposited on silica spheres modified by polyelectrolyte layers. Subsequent HF treatment yields hollow FePt spheres. Interestingly, the magnetic properties of annealed hollow spheres can be tailored from soft to hard magnetism, depending on annealing conditions. Polymer spheres (e.g., polystyrene and polymethylmethacrylate) are also used as a template material to create hollow structured materials.[122] In this case, polymer cores are removed from sonochemically produced composites by either thermal pyrolysis or extraction with organic solvents.

© 2010 WILEY-VCH Verlag GmbH & Co. KGaA, Weinheim

2.2.5. Carbons

Sonochemistry offers an alternative synthetic route to prepare various nanostructured carbon materials (e.g., carbon nanotubes, nano-onions, nanoscrolls, etc). While traditional synthetic methods for such carbon nanostructures require harsh conditions (e.g., high temperature, high vacuum, high-voltage arc discharge, or high-energy electron beam), the newly developed sonochemical route can be carried out under ambient conditions (e.g., room temperature and atmospheric pressure) and sometimes even without the use of a metal catalyst.[123]

Teo and coworkers synthesized hydrocarbon nanotubes and nano-onions by sonicating a suspension of HF-etched Si nanowires in common organic solvents (e.g., $CHCl_3$, CH_2Cl_2, CH_3I, etc.).[123,124] Ultrasonic irradiation enhances the reactions between SiH_x species and organic molecules (i.e., elimination of substituents on the solvent molecules), resulting in exotic carbon nanostructures. Park and colleagues reported the sonochemical preparation of single-walled carbon nanotubes.[125] In this novel synthetic strategy, ferrocene was used as the source of an Fe catalyst, and silica powder and *p*-xylene were utilized as a nucleation site and a carbon source, respectively. The extreme conditions created by acoustic cavitation aid in the decomposition of ferrocene and *p*-xylene and provide sufficient energy for the growth of high-purity carbon nanotubes from the Fe catalyst on the surface of silica powder. In addition to its ambient reaction conditions (i.e., room temperature and atmospheric pressure), this sonochemical process eliminates extra purification processes, opening the possibility of using this method for large-scale production of high-purity carbon nanotubes.

Besides the direct synthesis of carbon nanostructures from a precursor, ultrasound can induce dramatic morphology changes in pre-synthesized carbon materials. Kaner and coworkers discovered that sonicating a dispersion of exfoliated graphite in ethanol yields carbon nanoscrolls (Figure 12) with a high conversion efficiency of 80%.[126] Control experiments revealed that sonication is essential for the nanoscroll formation.

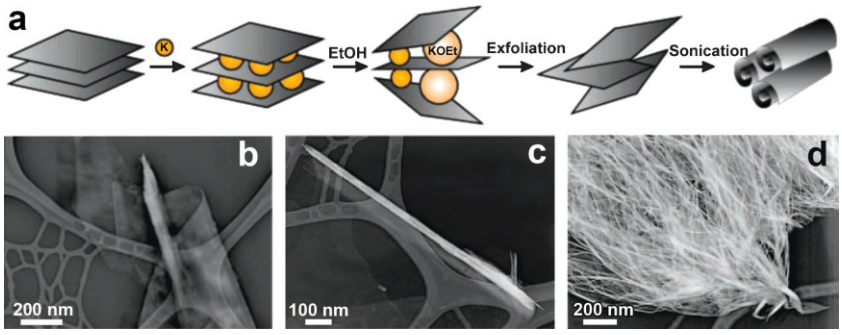

Figure 12. a) Schematic of the intercalation/exfoliation process. Graphite is intercalated with potassium metal and then exfoliated with ethanol (EtOH) to form a dispersion of carbon sheets. Sonication produces carbon nanoscrolls. TEM images of b) a thin plate of graphitic sheets in the process of scrolling, c) an isolated carbon nanoscroll with open ends, and d) a mass of scrolled material, representative of the bulk of the sample. The lighter web pattern in the background of each image is the lacey carbon TEM grid. Reproduced with permission from [126]. Copyright 2003, AAAS.

2.2.6. Sonochemical Preparation of Protein and Polymer Nano and Microstructures

Applications of ultrasound to materials chemistry have been further developed for biomaterial synthesis, and continually extended to polymers as well.[19] While we will not review this in depth (due to space limitations), we will mention a few highlights. Suslick and coworkers pioneered sonochemical synthesis of protein microspheres, where simple sonication of a protein solution (e.g., serum albumins) produces microcapsules filled with air or a nonaqueous liquid.[127–134] These biocompatible and stable microspheres are of particular interest in various biomedical applications including their FDA approved use as contrast agents for magnetic resonance imaging (MRI), sonography, and optical coherence tomography (OCT) as well as oxygen or drug delivery carriers. In-depth mechanistic studies revealed that the combined acoustic phenomena, emulsification and cavitation, account for microsphere formation: short-lived protein microspheres (usually of serum albumin) generated by ultrasonic emulsification gain greatly improved stability via covalent disulfide cross-linking of cysteine residues, for which sonochemically generated hydroperoxyl radicals (i.e., protonated superoxide, $HO_2\cdot$) are primarily responsible.[127,128,133] As shown by circular dichroism studies, the emulsification process does not lead to any significant degradation or denaturing of the protein molecules in the microsphere shells.[127,128] In addition to the covalently cross-linked albumin microspheres, sodium polyglutamate (SPG) microspheres have recently been reported that are stabilized by hydrogen bonding networks instead of covalent cross-linking.[134]

In addition to biopolymers, sonochemically generated radicals have been utilized to produce various organic polymers.[19,135,136] For instance, Grieser and coworkers recently reported sonochemically produced polymer latex nanoparticles doped with fluorescent and phosphorescent dyes.[136] Ultrasound-induced radical emulsion polymerization can have several advantages over a conventional chemically- or thermally-initiated polymerization: facile production of nanometer-sized particles, a lower surfactant concentration, and room temperature reaction conditions. The utilization of ultrasonic irradiation in the synthesis of inorganic polymers has been also examined by several research groups.[19] Matyjaszewski et al. sonochemically synthesized polysilanes with monomodal high molecular weight distributions at ambient temperatures.[137] Sonicating nonpolar aromatic solutions of silane monomers in the presence of sodium yields polysilanes with low polydispersity ($M_w/M_n < 1.2$).

3. Ultrasonic Spray Pyrolysis

In contrast with sonochemistry, where ultrasound directly induces chemical reactions, in USP, the ultrasound is *not* directly employed in chemical reactions, which are in fact thermally driven. Instead, the role of the ultrasound in USP is to provide the phase isolation of one microdroplet reactor from another. While high intensity ultrasound with a low frequency (typically 20 kHz) is used in sonochemistry, USP generally utilizes lower intensity ultrasound with a high frequency (e.g., ~2 MHz). In USP, ultrasound

WILEY InterScience DISCOVER SOMETHING GREAT
© 2010 WILEY-VCH Verlag GmbH & Co. KGaA, Weinheim

nebulizes precursor solutions to produce the micron-sized droplets that act as isolated, individual micron-sized chemical reactors. Both cavitation-induced sonochemistry and USP, in general, are involved phase-separated (i.e., two- and sometimes multi- phase) chemical reactions. In USP, liquid droplets generated by ultrasonic nebulization are heated in a gas flow, and subsequently solid-phase or sometimes liquid-phase (when precursors melt prior to decomposition or when high boiling point liquids are used) chemical reactions occur. The major differences between two synthetic methods are summarized in Table 1.

Spray pyrolysis has been widely used in industry for ultrafine- and nanoparticle production as well as film deposition, in part because the apparatus is simple and continuous and can be scaled easily for mass production. In general, spray pyrolysis involves the thermal decomposition of aerosols (i.e., solid or liquid particles suspended in a gas) generated by an nebulizer (e.g., pneumatic, ultrasonic, or electrostatic nebulizers) in a gas flow.[138] Among the various nebulization techniques, the use of ultrasonic nebulizers has been favored because of their outstanding energy-efficiency in aerosol generation over other nebulization tools, affordability (e.g., the use of household humidifiers), and the inherently low velocity of the initial aerosol. As a synthetic tool, USP has several advantages over other traditional methods: production of micron- or submicron-sized spherical particles, high product purity, continuous operation, and ease of controlling composition.[138–140] Unlike conventional solid- or liquid-phase synthetic methods (e.g., precipitation, hydrothermal method, and solid-state reaction) where batch reactions are performed to produce materials, the USP technique is a continuous flow process that enables both large and small scale production of products with excellent reproducibility. In addition, the facile control over chemical and physical compositions in the USP method makes USP particularly useful in the preparation of multicomponent or composite materials.[138]

The droplet formation by low frequency ultrasound was first described by Wood and Loomis in 1927.[141] In 1962, Lang experimentally established the relationship between ultrasonic frequency and droplet size.[142] Ultrasonic nebulization (Figure 13) is a result of capillary waves (i.e., waves travelling along the interface between two fluids) at the surface of liquids; in other words, nebulization is a result of momentum transfer. The capillary waves generated by ultrasonic vibrations at the liquid's surface consist of crests and troughs. When the amplitude of the surface capillary waves is sufficiently high, the crests (peaks) of the capillary waves can break off, resulting in liquid droplets. Since the capillary wavelength is inversely proportional to frequency, finer droplets can be produced at higher frequencies. Several other parameters (e.g., surface tension and density) also affect the droplet size along with frequency, which is well-described by the Lang equation:[142]

$$D_{droplet} = 0.34\left(\frac{8\pi\gamma}{\rho f^2}\right)^{1/3} \quad (8)$$

where D is mean droplet diameter, γ (N m^{-1}) is surface tension, ρ (kg m^{-3}) is solution density, and f (MHz) is the ultrasonic frequency. For nanomaterial synthesis, high frequencies (e.g., >1 MHz) are generally used, but commercial large scale nebulizers are also available in the 25 kHz region and are used for spray drying and painting.

A typical USP apparatus consists of an ultrasonic transducer at the base of a vessel containing precursor solutions and fitted with a gas stream to carry the mist into a tubular furnace; a collector is positioned at the furnace outlet (e.g., bubbler, filter, electrostatic precipitator, etc); for film deposition, substrates such as silicon and glass are usually placed inside the furnace (Figure 14a). The liquid droplets generated by ultrasonic nebulization are carried through a heated zone by a gas flow (e.g., Ar, N_2, O_2, etc). Often,

Table 1. Comparison of the complementarities of sonochemistry and ultrasonic spray pyrolysis. Images: multi-bubble sonoluminescence in 85 wt% phosphonic acid and ultrasonic mist produced at 1.7 MHz, respectively.

	Sonochemistry	Ultrasonic spray pyrolysis
	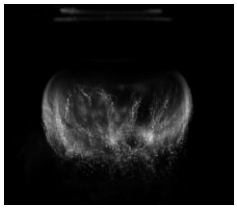	
Reaction site	Gas bubbles	Liquid microdroplets
Conditions	~5000 K, 1000 bar	500–1300 K, 1 bar
Reactants	Volatiles primarily	Nonvolatile solutes
Cooling rates	$>10^{10}$ K s^{-1}	10^4 K s^{-1}
Templating	Easy	Easy, easy nanocomposites
Heating zone	Single extreme hot zone	Multiple hot zones possible
Scalability	Scalable: kg/day	Easily scalable: ton/day
Particle size control	Nano- and submicron-sized particels	Typically submicron-size, but nanoparticles possible
Composition control	Easy	Easy
Anisotropic shapes	Yes	No
Hollow structures	Yes	Yes
Core/shell structures	Yes	Yes

© 2010 WILEY-VCH Verlag GmbH & Co. KGaA, Weinheim

Figure 13. Photograph of an ultrasonic fountain and mist produced at 1.7 MHz. Reproduced with permission from [191]. Copyright 2005, American Chemical Society.

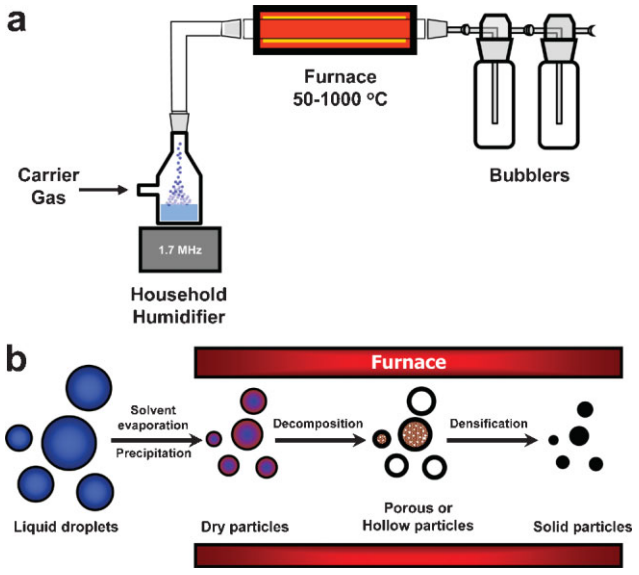

Figure 14. Schematic illustration of (a) typical USP apparatus and (b) a simplified USP process. Adapted with permission from [138].

additional furnaces are attached to the end of the single furnace to increase residence time of the droplets in the heated zone or to achieve multi-zone temperatures. In a laboratory-scale USP rig used in the Suslick research group, for example, an inexpensive high frequency ultrasound generator from a household humidifier can be used to create a useful source for USP, eliminating the need for expensive, commercial ultrasonic nebulizers.

The USP synthetic process involves droplet generation, evaporation of solvents, diffusion of solutes, precipitation, decomposition, and densification (Figure 14b).[138] The entire USP process, however, is more complicated, and some of the processes are still poorly understood. A simplified and qualitative description of the USP process will be discussed here; more detailed descriptions are available in several excellent books and reviews.[138–140,143,144] The first process that occurs during USP is the formation of liquid droplets by ultrasonic nebulization. As previously mentioned, the size of the droplets can be controlled by changing several parameters, but typically, in the case of water, spherical droplets with an initial diameter of ~5 μm are obtained at a frequency of ~2 MHz. The liquid droplets are then carried into a heated zone by a gas flow with subsequent solvent evaporation from the surface of the droplets. During solvent evaporation, the droplets rapidly shrink, and further heating leads to supersaturation, at which point precipitation of solute takes place, often at the surface of the droplet. Decomposition of precursors may follow to produce porous or hollow intermediate particles, which may subsequently undergo densification to yield solid particles. The formation of dense solid particles versus hollow shells is intimately related to solvent evaporation rate and solubility of precursors.[138,140,143] These factors can affect the degree of supersaturation, which significantly influences the morphology of final products.

3.1. Preparation of Fine Powders and Films

USP has proven to be a versatile technique for the preparation of fine powders (i.e., micron-sized) of metals, metal alloys, and ceramic materials. A number of examples of metals and their alloys (e.g., Ag,[145] Pd,[146] Au,[147] Cu,[148] Ni,[149] Co,[150] and Ag–Pd[151]) production have been reported. Typical syntheses to produce metal or alloy particles involve a simple decomposition of aqueous metal salt (typically nitrate) solutions under an inert gas flow (e.g., N_2 or Ar). Sometimes, especially when producing non-precious metal particles (e.g., Cu, Ni, or Co), the carrier gas is switched to H_2 to provide a reducing environment during USP.[148–150,152] Instead of flowing hydrogen gas, in situ generated H_2 has also been utilized to produce non-precious metal particles; Ehrman and coworkers found that adding an alcohol co-solvent such as ethanol into precursor solutions can create a strong reducing environment from the thermolysis of ethanol to CO, H_2, and CH_4.[148,152] Rao and colleagues extended this synthetic procedure to prepare single crystalline Zn, Cd, Co, and Pb nanowires.[153] In this synthesis, methanolic solutions of metal acetates were employed to produce metal nanowires.

Myriads of micron-sized powders of metal oxides (e.g., mono-metallic oxides and multi-component or composite materials) and metal chalcogenides have been synthesized via USP synthetic routes. In general, metal nitrates, chlorates, and acetates are employed as precursors; in case of metal chalcogenide synthesis, chalcogen sources are added to the precursor solution. As long as suitable precursors are available, fine powders of nearly any metal oxide or chalcogenide can be simply prepared using the USP method.[138,140]

WILEY InterScience DISCOVER SOMETHING GREAT
© 2010 WILEY-VCH Verlag GmbH & Co. KGaA, Weinheim

In addition, USP has found increased utilization in the synthesis of multi-component and composite powders. Liquid-phase precipitation, one of the most frequently used methods, often suffers in producing crystalline particles; the inevitable annealing at high temperatures to improve crystallinity, however, inherently leads to agglomeration. In contrast, hydrothermal synthesis can produce highly crystalline materials, but to date, its usefulness for the synthesis of multi-component and composite materials has been severely limited. Conventional solid-state synthesis, on the other hand, offers a facile route to produce a wide variety of crystalline materials, but has difficulties in controlling particle size and morphology, as well as severe agglomeration. Compared to these traditional synthetic methods, USP has an excellent ability to control chemical composition and morphology as well as to produce non-agglomerated, crystalline particles because of its unique reaction conditions (i.e., isolated, micron-sized chemical reactors). The usefulness of multi-component and composite materials prepared by USP has been found in a variety of applications including field emission displays, lithium batteries, solid oxide fuel cells, catalysis, and superconductors.[154–165]

Since its first use in 1966 for CdS film deposition as solar cells,[166] the utilization of the USP technique in this field has become increasingly widespread. Along with its simplicity and versatility, USP has several advantages over other techniques: facile doping, wide ranging substrate materials or dimensions, precise control over film thickness and composition, and moderate operating temperatures. Many successful examples of USP in thin film deposition are easily found in the literature.[138,144]

3.2. Preparation of Nanostructured Materials by USP

Despite the advantages of the USP technique, its utilization had long been confined to the production of micron-sized powders and thin films. During the last 10 years, however, USP has been revived by several research groups as a generalized synthetic method for the preparation of nanostructured materials. This conspicuous transformation of the USP technique into a powerful synthetic tool has originated from its outstanding ability to produce nanocomposites. In a majority of cases, the nanocomposites are composed of desired materials (e.g., metal oxides, sulfides, or carbon) combined with sacrificial materials (e.g., surfactants, colloidal silica, polymers, or metal salts). The sacrificial materials are subsequently removed by several methods (e.g., chemical etching, calcination, or dissolution), introducing various nanostructures (e.g., porosity) into final products. In the following discussion, various nanostructured materials prepared by USP will be grouped into several categories based on the nature of the sacrificial materials.

3.2.1. Nanostructured Materials from Organic-Inorganic Hybrid Nanocomposites

Mesostructured framework solids consist of nanometer-sized, thin walls integrated continuously in an orderly fashion. Well-ordered mesoporous materials often have unique properties with important applications to catalysis, sorption, gas sensing, optics, and photovoltaics.[167–169] Often, the physical and chemical properties of the well-ordered mesoporous materials are significantly different from their nonporous, solid counterparts.[170] Typical synthetic procedures for mesostructured materials are batch reactions where self-assembled organic-inorganic hybrid nanocomposites are produced with the assistance of pre-organized organic species (e.g., surfactants and amphiphilic block copolymers), which are then burnt out of the final mesoporous material.

Despite their versatility and reproducibility, the batch synthetic routes possess several critical drawbacks: tedious and time-consuming templating processes, difficulties of their use to produce thin films, and limited utilization for the production of patterned nanocomposites.[171] Brinker and coworkers addressed such problems by combining an evaporation-induced self-assembly (EISA) process and aerosol techniques.[172,173] In this pioneering work, they sprayed homogeneous water/ethanol mixture solutions containing silica precursors and surfactants whose initial concentrations were considerably less than the critical micelle concentration into a heated zone. As the aerosol droplets are heated in the furnace, rapid solvent evaporation takes place, causing the surfactant concentration to exceed the critical micelle concentration at the droplet surface. Further solvent evaporation renders the entire surfactant concentration greater than the critical micelle concentration throughout the droplet, initiating micelle formation. The micelles subsequently organize into liquid-crystalline mesostructures. Strictly speaking, this synthetic process should not be called USP because no decomposition (i.e., pyrolysis) is involved in this aerosol process; rather, this is more accurately an aerosol-assisted sol-gel reaction.

Heat-treatment (i.e., calcination under oxygen) of the obtained organic-inorganic hybrid nanocomposites produces various forms of mesostructured silica spheres, depending on the

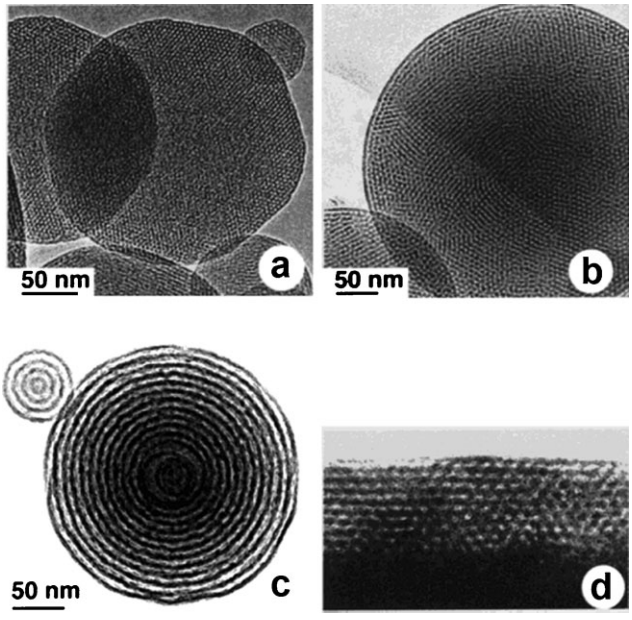

Figure 15. Representative TEM images of mesostructured silica particles and film. (a) faceted, calcined silica particles with a hexagonal mesophase; (b) calcined silica particles showing cubic mesostructure; (c) calcined particles showing a vesicular mesophase; (d) cross-section of porous silica film deposited on a silicon substrate. Reproduced with permission from [171].

© 2010 WILEY-VCH Verlag GmbH & Co. KGaA, Weinheim

surfactant used in the synthesis (Figure 15a–c).[172] For instance, when cetyltrimethylammonium bromide (CTAB), a cationic surfactant, was used as a structure-directing agent, spherical particles with a highly ordered hexagonal mesophase were produced. Non-ionic surfactants (e.g., Brij-56 or 58), on the other hand, produced silica particles showing a layered, vesicular mesostructure. Interestingly, adding swelling agents (e.g., polypropylene glycol dimethylacrylate and polypropylene oxide) into the precursor solutions gave control over the mesopore diameters.[174] Along with the powder production, this aerosol-assisted synthetic route proved to be very useful even for the formation of ordered mesostructured thin films (Figure 15d); the droplet coalescence on substrates results in the formation of uniformly well-ordered thin films.[175]

Another advantage of this synthetic route is the ability to incorporate metal species, organic dye molecules, or polymers within the mesostructured framework.[172,176–179] With metal complexes added to precursor solutions, for instance, metal/silica nanocomposites (e.g., gold/silica and palladium/silica) can be easily obtained.[172,176] Simultaneous control over metal loadings and pore structures provides sophisticated level of control with this synthetic approach unavailable through other conventional methods such as incipient wetness. Lu and coworkers also demonstrated that encapsulating polymers into a silica framework via the aerosol route is a facile method for the preparation of mesoporous carbon nanocapsules.[180]

Several other groups have extended the aerosol procedure developed for mesostructured silica particles to prepare other mesostructured metal oxides. Grosso and coworkers reported crystalline, mesoporous γ-alumina with high thermal and chemical stability via this route.[181] Very recently, Wang and colleagues synthesized rare-earth-doped, mesoporous titania microspheres.[182] Not only does the aerosol process enable multiple rare earth ion doping (e.g., Eu^{3+} and Sm^{3+}) but it also permits a simple change in their ratios and results in tunable, multiple photoluminescence emission.

3.2.2. Nanostructured Materials from Silica-based Nanocomposites

Hard templates, especially colloidal silica, have also proven useful in the USP preparation of nanostructured materials. Silica nanoparticles will close-pack in an evaporating droplet and can provide a nanostructured scaffold in situ.

Suslick and Skrabalak utilized silica particles as a sacrificial component in USP-produced nanocomposites to prepare porous MoS_2 via USP.[183] While USP without templating produces only submicron-sized, spherical solid MoS_2 spheres, USP with templating yields SiO_2/MoS_2 nanocomposite from the decomposition of a single-source MoS_2 precursor dissolved in an aqueous suspension of nanometer-sized, colloidal silica particles. Subsequent HF etching selectively leaches silica nanostructures out of the nanocomposite, resulting in porous MoS_2 network. The nature of the resulting MoS_2 nanostructure (e.g., porosity and surface area) can be easily tuned by changing the size and concentration of silica particles. The porous MoS_2 produced by the USP technique was shown to be an extremely active catalyst for hydrodesulfurization reaction compared to its nonporous counterpart. Upon doping with cobalt, the porous MoS_2 exhibits a superior catalytic activity and selectivity than even RuS_2, known as the most intrinsically active catalyst for hydrodesulfurization.

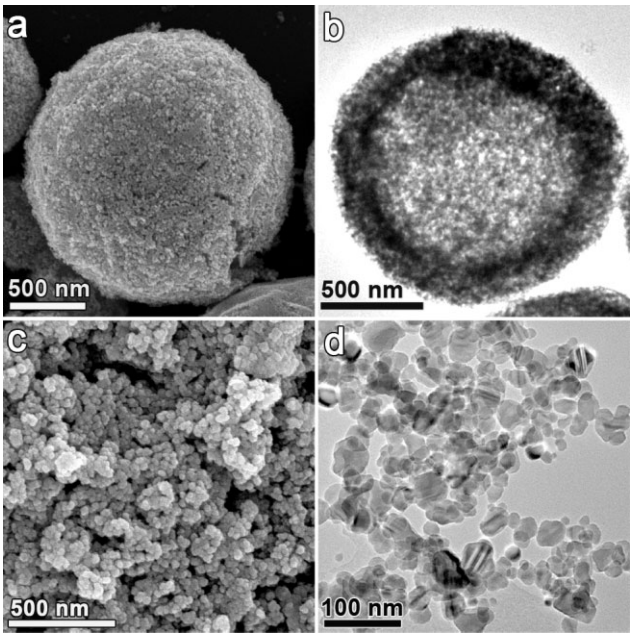

Figure 16. Electron micrographs of nanostructured ZnS:Ni^{2+} hollow microspheres and nanoparticles produced by USP. Reproduced with permission from [184].

Recently, nanostructured ZnS:Ni^{2+} photocatalysts were prepared in a similar manner and evaluated for hydrogen evolution under visible light (Figure 16).[184] Because of their high energy conversion efficiency and the relatively negative redox potential of their conduction band, ZnS photocatalysts have been examined for a variety of applications, including degradation of water pollutants, reduction of toxic heavy metals, and water-splitting for H_2 evolution. In the USP synthesis of ZnS:Ni^{2+} photocatalysts, mesoporous hollow microspheres (Figure 16a and b) were obtained at a low temperature after silica template removal, whereas nanoparticles (Figure 16c and d) are produced at a high temperature. This temperature-dependent morphology change is related to the rapid crystal growth of ZnS at high temperatures, which results in ZnS nanoparticles larger than the silica colloid template; such composites are not sufficiently strongly held together to sustain the hollow microsphere structure after the silica template is removed. In addition to the rapid crystal growth, gas released during the decomposition of the ZnS precursors may also lead to the destruction of the porous microspheres. Photocatalytic activity of USP products of ZnS:Ni^{2+} toward water-splitting under visible light was examined in the presence of sacrificial electron donors (K_2SO_3 and Na_2S). The most efficient of the ZnS:Ni^{2+} morphologies are nanoparticles, which are well-balanced between crystallinity and surface area. The USP nanoparticles were further compared to conventional powders, and it was found that the photocatalytic activity of the USP nanoparticles for H_2 production is substantially superior to those of ZnS:Ni^{2+} powders. These results clearly demonstrate that USP is a robust and efficient method for production of highly active photocatalysts.

WILEY InterScience DISCOVER SOMETHING GREAT
© 2010 WILEY-VCH Verlag GmbH & Co. KGaA, Weinheim

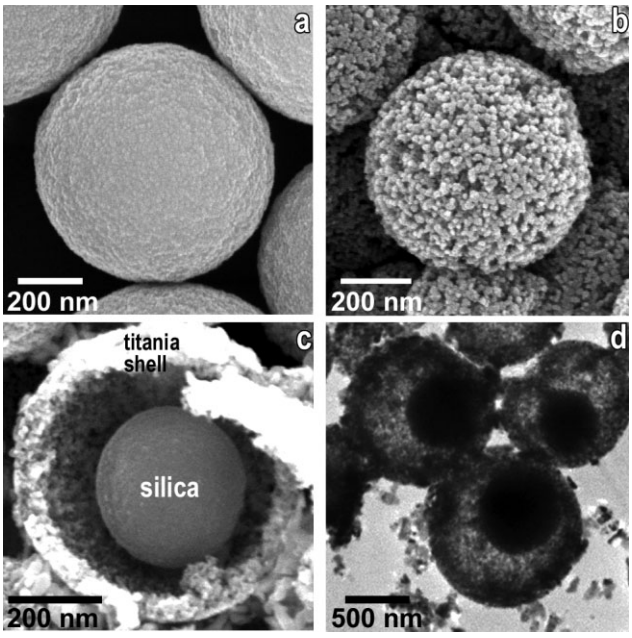

Figure 17. Electron micrographs of (a) silica-titania composite produced by USP and (b) porous titania obtained by HF treatment; (c) SEM and (d) TEM image of ball-in-ball silica-titania composite decorated with Co oxide nanoparticles after partial etching with HF. Reproduced with permission from [185].

The utilization of a silica template has been further extended for the synthesis of nanostructured metal oxides. Suslick and coworkers reported the USP synthesis of various forms of titania nanostructures, including porous, hollow, and ball-in-ball architectures (Figure 17).[185] When an aqueous solution containing a titanium complex and silica nanoparticles is nebulized and decomposed via the USP process, a titania/silica nanocomposite is produced (Figure 17a). This normally produces a porous titania microsphere after the silica is selectively etched with HF from the nanocomposite (Figure 17b). In the presence of some transition metal ions in the precursor solution, however, an unusual phase separation occurs during USP with the formation of an outer titania enriched shell and an inner silica core. Upon etching, this generates initially a ball-in-ball with an inner silica core and an outer porous titania shell (Figure 17c and d); on full etching, the core is gone and only a porous titania spherical shell remains; the exact mechanism by which the transition metal ions induce the phase separation remains unknown. Cytotoxicity studies revealed that these nanostructured microspheres possess negligible effects on the viability of various cell lines, which led to the further examination of these materials as potential drug delivery agents. The microspheres loaded with a potential drug for Alzheimer's disease showed an outstanding ability to selectively deliver the drug to cytosol rather than cell nuclei.

In another use of silica colloid templating, Lu and coworkers synthesized various kinds of porous carbon spheres from silica/sucrose nanocomposites.[186,187] By changing the type of silica template and manipulating the ratio of template to sucrose, they were able to simply control the pore structures of carbon spheres and their macroscopic morphology. Hydrogen physisorption on these carbon materials has been recently evaluated, presenting a potential use of these USP carbons for hydrogen storage applications.[187]

3.2.3. Nanostructured Materials from Polymer-based Nanocomposites

Colloidal polymer particles have also been utilized as a template material in USP synthesis. Okuyama and coworkers synthesized ordered macroporous (i.e., pores with diameters of >50 nm) silica spheres by employing polystyrene latex particles as a template.[188,189] In this approach, a dilute colloidal suspension of silica and polystyrene latex is ultrasonically nebulized, and the resulting droplets are carried though heating zones with a temperature gradient. The droplets first pass through a low-temperature zone where a silica/polystyrene nanocomposite is created after solvent evaporation, and in the subsequent high-temperature zone the polystyrene particles of the intermediate nanocomposite are pyrolyzed out as gases, leaving ordered macroporous silica spheres behind. Occasionally an additional, higher temperature zone is added to anneal the porous silica in situ.

As with colloidal silica templating, the polymer particles tend to organize into an ordered network during solvent evaporation. In this case, polystyrene particles are packed in a hexagonal fashion, and the choice of polystyrene particle size changes the pore size of the resulting porous silica spheres. When colloidal silica nanoparticles are replaced with titania nanoparticles, macroporous titania spheres are simply obtained; the Okuyama research group recently reported[190] macroporous, brookite titania spheres using the same synthetic route and demonstrated an enhanced photocatalytic performance of these porous spheres, resulting from their large surface area and improved resistance against sintering during photochemical reactions.

One would wish to combine the macroporosity resulting from a polymer template and the mesoporosity achieved by surfactant self-assembly. Brinker and coworkers exploited colloidal polystyrene particles and a surfactant as a structure-directing agent for macroporosity and mesoporosity, respectively.[174] The combination of two different templates turned out to be very effective for creating multiple-sized pores in silica spheres, which are interconnected to each other, and even controlling the pore structures.

The polymer templating strategy has been further developed by Suslick and Suh who utilized an in situ generated polymer template for the preparation of macroporous silica spheres (Figure 18).[191] While the polymer templating method originally developed by the Okuyama research group is robust and simple, it relies on the use of expensive polymer beads for the creation of macroporosity. In Suh's method, however, the polymerization of an organic monomer (i.e., styrene) in the nebulized droplets having silica nanoparticles takes place at the first heating zone held at a low temperature, creating a silica/polystyrene nanocomposite in situ. The nanocomposite is then carried into a second, hotter temperature zone where the in situ generated polymer is pyrolyzed out, producing macroporous silica spheres. The morphology and surface area of the porous silica spheres are also easily controllable by manipulating the ratios of styrene and

© 2010 WILEY-VCH Verlag GmbH & Co. KGaA, Weinheim

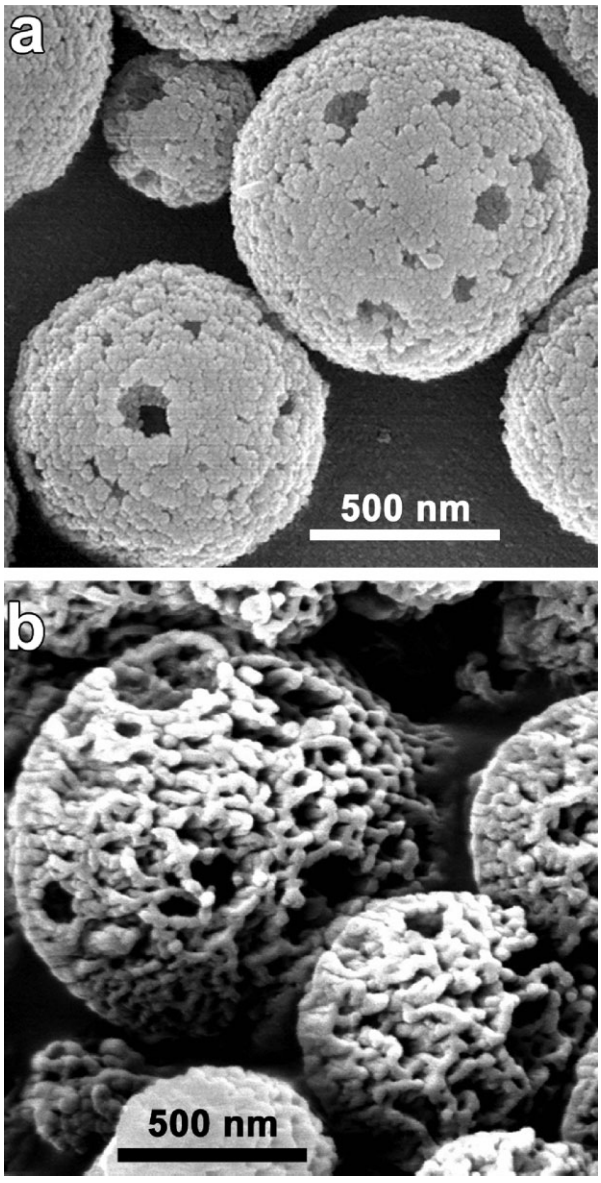

Figure 18. a) SEM images of macroporous silica spheres produced by USP and b) their wormhole-like inner structure. Reproduced with permission from [191]. Copyright 2005, American Chemical Society.

silica. Furthermore, upon $Co_2(CO)_8$ addition to the precursor solutions, the resulting porous silica spheres can possess ferromagnetism, which originates from the $Co_2(CO)_8$ decomposition product encapsulated in the silica matrix (Co nanoparticles). Magnetic studies revealed that the porous silica matrix effectively shields the Co nanoparticles from oxidation, allowing the cobalt/silica composite to retain their initial magnetism >6 months.

3.2.4. Nanostructured Materials from Metal Salt-based Nanocomposites

In the traditional USP process, one initial droplet yields one final particle. While multiple nucleation occur at an early stage of the USP process, the resulting multiple nanocrystallites grow and aggregate into a larger micron-sized single particle as thermal heating in the droplet proceeds. This distinctive nature of the USP process has excluded the use of USP for the production of nanoparticles. There have been some attempts to produce nanometer-sized particles by USP (e.g., low-pressure spray pyrolysis);[192–194] however, the requirement of a vacuum system and the difficulties in controlling experimental parameters in this method have prevented its wide spread use for nanoparticle production.

To address such issues, Okuyama and coworkers proposed a facile, rapid, and generalizable USP method. In their synthetic strategy named ''salt-assisted aerosol decomposition'', metal salts (e.g., chlorides or nitrates of Li, Na, K) or their eutectic mixtures are simply introduced into precursor solutions to prevent the agglomeration of nanocrystallites produced at the early stage of USP process.[195] The added metal salts play a role as hot liquid solvents where nanocrystallites can dissolve and precipitate during USP process. Such multiple series of dissolution/precipitation events occurring in the molten droplets lead to the production of separated nanoparticles trapped in a salt matrix. The molten salts and the non-agglomerated nanoparticles then solidify as the aerosol droplets are cooled, and the salt matrix is subsequently removed by several cycles of washing, resulting in separated nanoparticles.

A wide variety of nanoparticles have been prepared, including Ni, Ag–Pd, NiO, CeO_2, ZnO, $LiCoO_2$, Y_2O_3–ZrO_2, $(Ba_{1-x}Sr_x)TiO_3$, CdS, and ZnS.[156,195–199] In addition to the versatility of this novel route, the molten salts serve as an effective liquid flux to improve mass transport.[195] Due to the greatly enhanced mass transfer rates, the materials produced via the salt-assisted aerosol decomposition method are often much more crystalline than the USP products obtained by the conventional USP method, which can improve their physical properties substantially.

Judicious control over the quantity of metal salts can create porous architectures (e.g., mesopores or hollow interiors) into the final USP products rather than producing fully separated nanoparticles. Zachariah and coworkers synthesized nanoporous metal oxides (e.g., Al_2O_3 and SiO_2) via Okuyama's synthetic approach.[200,201] Instead of using excess amounts of metal salts, they used intermediate concentrations of salts in the precursor solution so the structural integrity of nanocrystallites in USP nanocomposite can remain after salt-removal. This strategy to generate porous structures has some real advantages: the in situ templating with salts is inexpensive and non-toxic, the salts can be used with good thermal stability at very high temperatures, and it is even possible to recycle the metal salts.

Hollow interior formation via metal salt templating has also been reported. Brinker and Jiang synthesized mesoporous silica particles with NaCl cores via the aerosol-assisted self-assembly method.[202] In this synthesis, an aerosol process followed by calcination produces a nanocomposite with a cubic single crystal NaCl core surrounded by a mesoporous silica shell, and a subsequent washing procedure removes NaCl to create a hollow cubic cavity. It is argued that NaCl precipitation precedes self-assembly of the silica shell, which results in the eventual formation of the hollow core. Lu and coworkers employed ferric

WILEY InterScience DISCOVER SOMETHING GREAT
© 2010 WILEY-VCH Verlag GmbH & Co. KGaA, Weinheim

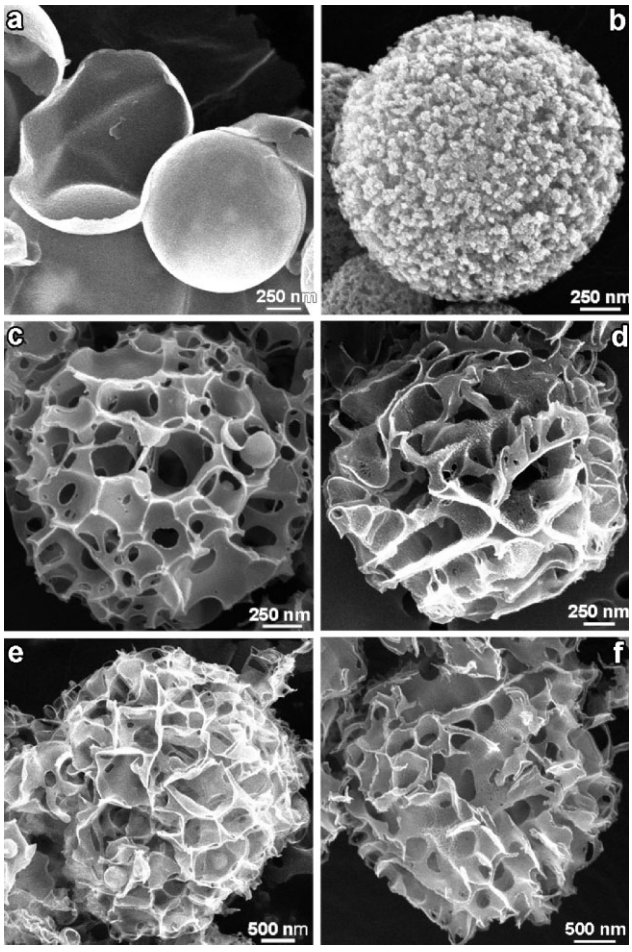

Figure 19. SEM images of USP porous carbons from various precursors: a) lithium chloroacetate, b) lithium dichloroacetate, and c) sodium chloroacetate, d) sodium dichloroacetate, e) potassium chloroacetate, and f) potassium dichloroacetate. Reproduced with permission from [204]. Copyright 2006, American Chemical Society.

chloride ($FeCl_3$) instead of sodium chloride (NaCl) to create hollow interiors.[203] In a similar manner, a nanocomposite with a ferric species-rich core surrounded by a silica-rich shell is produced, but interestingly, calcination of the nanocomposite results in a rattle-like nanostructure (i.e., hematite nanoparticles encapsulated in hollow silica spheres).

Unlike the salt-assisted methods discussed above where pre-existing metal salts are employed to create pore structures, a newly devised USP method for porous carbons utilizes in situ generated metal salts as a template. Suslick and Skrabalak reported USP synthesis of various nanostructured carbons from the decomposition of alkali halocarboxylates (Figure 19).[204] While traditional procedures for porous carbon synthesis require a series of tedious steps (e.g., creation of porous framework, infiltration of carbon precursors, carbonization, and template removal), the new approach is a one-step process and does not require relatively expensive template materials. Depending on the types of alkali halocarboxylates, a variety of nanostructures (mesoporous, macroporous, and hollow) are created (Figure 19a–f). For instance, the USP products of an aqueous solution of alkali metal chloroacetates (H_2ClCCO_2M, M = Li, Na, K) are hollow carbon spheres (Figure 19a) and macroporous carbon cages (Figure 19c–f), whereas the pyrolysis of a lithium dichloroacetate (HCl_2CCO_2Li) solution yields mesoporous carbon spheres (Figure 19b). In-depth studies on a decomposition pathway of precursor solutions (using differential scanning calorimetry and thermal gravimetric analysis) revealed that the formation of pore structures is intimately related to the relative order of precursor melting and decomposition processes. In case of mesoporous carbon shown in Figure 19b, for instance, the decomposition of lithium dichloroacetate generates LiCl, which then acts as a temporary pore template as carbon network growth occurs. In the macroporous carbon shown in Figure 19c–f, on the other hand, no melting occurs before precursor decomposition; as a result, the carbon network forms through solid-state reactions, resulting in macropore formation.

USP decomposition of aqueous solutions of substituted alkali benzoate salts also produced various porous or hollow carbon spheres.[205] Interestingly, the size of the carbon spheres is linearly correlated to the concentration of precursor solutions. In addition, both the cation and the ring substituents of a given precursor influence product morphology. In contrast with the porous carbons produced from the decomposition of alkali halocarboxylates, electron micrographs revealed that in situ generated salts do not account for pore or bowl formation, suggesting that their formation is involved in different mechanisms. Thermogravimetric analysis of precursors suggests that the relative temperature of decomposition steps releasing gas determines morphology differences.

Porous carbon powders produced by USP were evaluated as catalyst supports for a direct methanol fuel cell (DMFC) catalyst and as pore formers in a membrane electrode assembly (MEA).[206] The effect of these materials on unit cell performance was compared to traditional Vulcan XC-72 carbon nanoparticle powder. It has been demonstrated that the inclusion of these carbon microspheres in electrodes is a simple, effective way to facilitate the mass transport of air and methanol during fuel cell operation.

3.2.5. Semiconductor Nanoparticles from Chemical Aerosol Flow Synthesis

Despite the success of the salt-assisted aerosol decomposition method for nanoparticle production, it had remained a serious challenge to produce high quality semiconductor nanoparticles (or quantum dots). Traditional synthetic routes (e.g., high-temperature decomposition of organometallic compounds) in general require rapid nucleation through thermal or concentration spikes to produce monodispersed nanoparticles.[207] In this respect, USP would be a suitable synthetic approach because the rapid heating and cooling of nebulized droplets that occurs during the USP process (with a timescale of seconds) can easily create the rapid nucleation required. Despite this potential advantage of USP method, however, the production of highly luminescent quantum dots via the USP route had not been realized until recently, mainly because of the use of aqueous precursor solutions in semiconductor preparation.[208]

© 2010 WILEY-VCH Verlag GmbH & Co. KGaA, Weinheim

To address this long-standing problem, Didenko and Suslick proposed a novel synthetic concept named "chemical aerosol flow synthesis",[209] using organic solutions of high boiling point liquids (e.g., octadecane) containing nanoparticle precursors instead of aqueous precursor solutions. Prior to ultrasonic nebulization, the organic precursor solutions are diluted with a low boiling point liquid (e.g., toluene) to make them less viscous. Nebulized droplets of the organic solutions first lose the low boiling point solvent as they pass through a heating zone, leaving a concentrated precursor solution in the high boiling point solvent behind. At this point, chemical reactions take place *in high boiling point organic liquid* to produce highly crystalline nanoparticles, and the reactions are then rapidly quenched in cold, solvent-filled bubblers. Highly fluorescent Cd-based quantum dots (e.g., CdS, CdSe, and CdTe as well as mixed chalcogenides) have been successfully prepared via this method (Figure 20a), and their particle size and consequently their photoluminescent emission can be easily tuned by simply changing the furnace temperature (Figure 20b). With this approach, one droplet is capable of yielding thousands of nanoparticles and high boiling point liquids containing surfactants prevent the agglomeration of nanoparticles. In addition, highly reproducible, gram-scale synthesis became possible (with a production rate of ~100 mg/h even with a laboratory-scale experimental setup), which had been significant limitations with traditional syntheses of quantum dots.

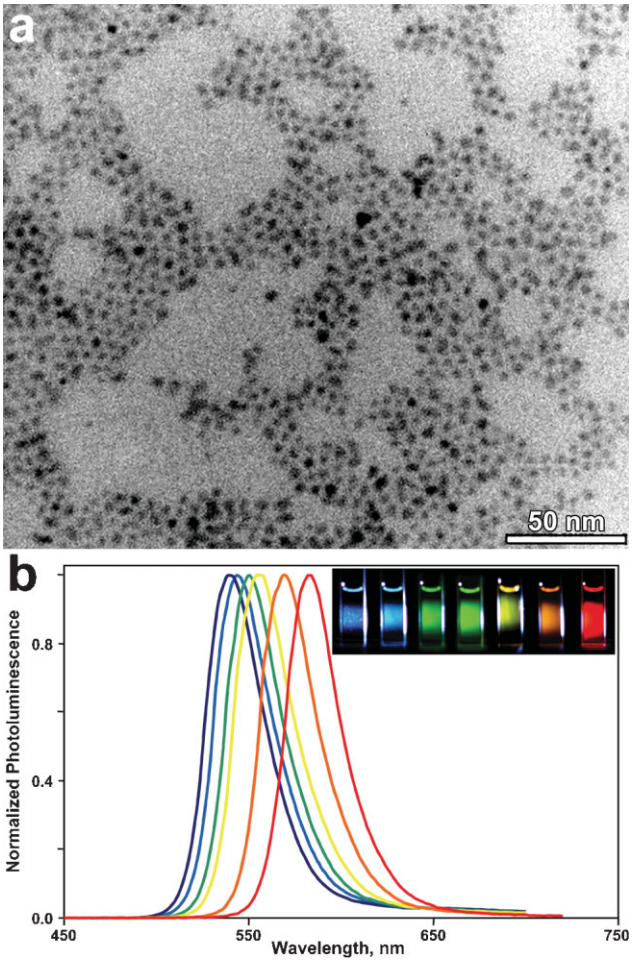

Figure 20. a) TEM image of CdSe QDs produced by USP at 340 °C and b) photoluminescence spectra of CdSe QDs obtained at temperatures of 240, 260, 280, 300, 320, and 340 °C (from left to right) in toluene solution (Inset: photograph of photoluminescence of the corresponding QDs in toluene solution). Reproduced with permission from [209]. Copyright 2005, American Chemical Society.

Very recently, this synthetic method has been further extended to prepare ternary CdTeSe and CdTeS quantum dots emitting at far-red and near-infrared (NIR) wavelength regions.[210] Far-red and NIR emitting QDs have the advantage that in biological systems the NIR is a clear window for in vivo imaging because autofluorescence, light absorption, and scattering from cells and cellular components is minimized. In the previous report,[200] CdTe nanocrystals stabilized by octadecylphosphonic acid (ODPA) with ~40% quantum efficiency had been successfully synthesized; the emission, however, could not be shifted further into the red than ~610 nm. The strong coordination bond in Cd-ODPA precursors significantly decreases the reactivity of the monomers, and the residence time of aerosolized precursors during the flow synthesis was insufficient for CdTe QDs to grow to the large-sized particles necessary for far-red and NIR emission. Furthermore, it has been noted that the stability of the ODPA-stabilized CdTe QDs in air is relatively poor compared to the fatty-acid-coated QDs. In this recent study, oleic acid was used as a stabilizer instead of octadecylphosphonic acid to provide greater stability. Also, upon adding a third element (Se) to the CdTe precursor solution and changing the reaction temperature, the photoluminescence of CdTe can be tuned from red to near-IR. The quantum efficiency of CdTe QDs was greatly improved by adding sulfur instead of selenium to the precursor solution because of better surface passivation of the CdS outer shell, which is grown during the flow synthesis over the initially formed CdTe core.

4. Conclusions and Future Outlook

A diverse set of applications of ultrasound have been explored in the synthesis of nanostructured materials, including both direct sonochemical reactions and ultrasonic spray pyrolysis. Ultrasonic irradiation provides unique reaction conditions via acoustic cavitation. Bubbles generated during sonication can effectively accumulate the diffuse energy of ultrasound, and upon collapse, an enormous concentration of energy is released to heat the contents of the bubble. These transient, localized hot spots with extremely high temperatures and pressures are primarily responsible for chemical effects of ultrasound. The usefulness of sonochemical synthesis as a synthetic tool resides in its versatility. With a simple modification in reaction conditions, various forms of nanostructured materials can be synthesized, including metals, alloys, oxides, sulfides, carbides, and nanostructured supported catalysts. The sonochemical method has been even further extended to the preparation of carbons, polymers, and biomaterials. Sonochemical decomposition of volatile organic precursors combined with significantly enhanced mass transport of materials via shock waves has been utilized in the synthesis of nanocomposites, often with a templating material

WILEY InterScience DISCOVER SOMETHING GREAT
© 2010 WILEY-VCH Verlag GmbH & Co. KGaA, Weinheim

as one component of the nanocomposites, and various hollow materials have been obtained after subsequent template removal. The applications of ultrasound in materials chemistry are diverse, and there still remains much to explore in the sonochemical synthesis of nanostructured materials. The major challenges that face a wider application of sonochemistry, however, include issues of scale-up and energy efficiency. While laboratory apparatus for sonochemical reactors is readily commercially available, larger-scale equipment remains relatively uncommon. Perhaps more importantly, sonochemistry shares with photochemistry an energy inefficiency that remains problematic: while the production of ultrasound from electrical power can be extremely efficient, the coupling of ultrasound into chemically useful cavitation events remains a low-yield event. As we begin to understand the physics of cavitation clouds and dense multiphase acoustics, more effective means of inducing cavitation in liquids may alleviate this current limitation.

In USP, on the other hand, ultrasound does not induce chemical reactions in and of itself. Instead, the ultrasound serves to nebulize precursor solutions producing micron-sized droplets that confine chemical reactions within their interior. Such phase-isolated micro-reactors allow for the facile control over chemical composition and complete retention of the bulk chemical composition on the micron-size scale. With these advantages, USP stands out among various synthetic routes for the preparation of multicomponent or composite materials. In spite of its several benefits, the development of the USP technique had long been stagnant. Substantial progress, however, with USP techniques has been achieved over the last 10 years, and USP has now been successfully revived as a generalized synthetic route for the preparation of nanostructured materials. The synthesis of nanostructured materials via USP-produced nanocomposites is robust and efficient, but there remains much room for further advancement. Despite the success in the preparation of high quality semiconductor nanoparticles via the chemical aerosol flow synthesis route, for instance, the current synthetic method is not easily adapted for the production of metal oxide nanoparticles because of short residence time of the microreactor droplets in furnace. In addition, the USP synthesis of nanostructured metal oxides is still limited to a few examples, in part because of the lack of suitable precursors for metal oxides and uncontrollably rapid sol-gel reactions. Considering the current limitations, future progress will require the development of new precursor materials and more systematical control over reaction parameters.

Acknowledgements

This work was supported by the U.S. Department of Energy, Division of Materials Sciences under Award No. DE-FG02-07ER46418, through the Frederick Seitz Materials Research Laboratory at the University of Illinois at Urbana-Champaign.

Received: November 30, 2009
Published online: February 1, 2010

[1] K. S. Suslick, *Ultrasound: Its Chemical, Physical, and Biological Effects*, Wiley-VCH, New York **1988**.
[2] K. S. Suslick, *Science* **1990**, *247*, 1439.
[3] K. S. Suslick, *Sci. Am.* **1989**, *260*, 80.
[4] K. S. Suslick, S. J. Doktycz, in *Advances in Sonochemistry*, Vol. *1* (Ed.: T. J. Mason), JAI Press, New York **1990**, pp. 197.
[5] H. Frenzel, H. Schultes, *Z. Phys. Chem.* **1934**, *27b*. 421.
[6] E. B. Flint, K. S. Suslick, *Science* **1991**, *253*, 1397.
[7] W. B. McNamara, III, Y. T. Didenko, K. S. Suslick, *Nature* **1999**, *401*, 772.
[8] Y. Didenko, W. B. McNamara, III, K. S. Suslick, *Nature* **2000**, *407*, 877.
[9] Y. T. Didenko, K. S. Suslick, *Nature* **2002**, *418*, 394.
[10] D. J. Flannigan, K. S. Suslick, *Nature* **2005**, *434*, 52.
[11] N. C. Eddingsaas, K. S. Suslick, *J. Am. Chem. Soc.* **2007**, *129*, 3838.
[12] D. J. Flannigan, S. D. Hopkins, C. G. Camara, S. J. Putterman, K. S. Suslick, *Phys. Rev. Lett.* **2006**, *96*, 204301.
[13] D. J. Flannigan, K. S. Suslick, *Phys. Rev. Lett.* **2005**, *95*, 044301.
[14] A. Weissler, *J. Am. Chem. Soc.* **1959**, *81*, 1077.
[15] A. Weissler, *Nature* **1962**, *193*, 1070.
[16] M. Anbar, I. Pecht, *J. Phys. Chem.* **1964**, *68*, 352.
[17] K. Makino, M. M. Mossoba, P. Riesz, *J. Am. Chem. Soc.* **1982**, *104*, 3537.
[18] K. S. Suslick, *MRS Bull.* **1995**, *20*, 29.
[19] K. S. Suslick, G. J. Price, *Annu. Rev. Mater. Sci.* **1999**, *29*, 295.
[20] A. Gedanken, *Ultrason. Sonochem.* **2004**, *11*, 47.
[21] K. S. Suslick, S. B. Choe, A. A. Cichowlas, M. W. Grinstaff, *Nature* **1991**, *353*, 414.
[22] M. W. Grinstaff, A. A. Cichowlas, S. B. Choe, K. S. Suslick, *Ultrasonics* **1992**, *30*, 168.
[23] K. S. Suslick, M. Fang, T. Hyeon, *J. Am. Chem. Soc.* **1996**, *118* 11960.
[24] J. Zhang, J. Du, B. Han, Z. Liu, T. Jiang, Z. Zhang, *Angew. Chem. Int. Ed.* **2006**, *45*, 1116.
[25] N. A. Dhas, C. P. Raj, A. Gedanken, *Chem. Mater.* **1998**, *10*, 1446.
[26] Y. Mizukoshi, R. Oshima, Y. Maeda, Y. Nagata, *Langmuir* **1999**, *15*, 2733.
[27] R. A. Caruso, M. Ashokkumar, F. Grieser, *Langmuir* **2002**, *18*, 7831.
[28] C. H. Su, P. L. Wu, C. S. Yeh, *J. Phys. Chem. B* **2003**, *107*, 14240.
[29] A. Nemamcha, J. L. Rehspringer, D. Khatmi, *J. Phys. Chem. B* **2006**, *110*, 383.
[30] K. Okitsu, K. Sharyo, R. Nishimura, *Langmuir* **2009**, *25*, 7786.
[31] K. Okitsu, M. Ashokkumar, F. Grieser, *J. Phys. Chem. B* **2005**, *109*, 20673.
[32] K. Vinodgopal, Y. He, M. Ashokkumar, F. Grieser, *J. Phys. Chem. B* **2006**, *110*, 3849.
[33] A. Brotchie, F. Grieser, M. Ashokkumar, *J. Phys. Chem. C* **2008**, *112*, 10247.
[34] S. Anandan, F. Grieser, M. Ashokkumar, *J. Phys. Chem. C* **2008**, *112*, 15102.
[35] A. Sánchez-Iglesias, I. Pastoriza-Santos, J. Pérez-Juste, B. Rodríguez-González, F. J. García de Abajo, L. M. Liz-Marzán, *Adv. Mater.* **2006**, *18*, 2529.
[36] I. Pastoriza-Santos, A. Sánchez-Iglesias, F. J. García de Abajo, L. M. Liz-Marzán, *Adv. Funct. Mater.* **2007**, *17*, 1443.
[37] L. P. Jiang, S. Xu, J. M. Zhu, J. R. Zhang, J. J. Zhu, H. Y. Chen, *Inorg. Chem.* **2004**, *43*, 5877.
[38] C. M. Wu, B. P. Zeng, T., *Chem. Mater.* **2006**, *18*, 2925.
[39] K. S. Suslick, M. Fang, T. Hyeon, A. A. Cichowlas, *Molecularly Designed Nanostructured Materials*, MRS Symp. Proc., K. E. Gonsalves, G. M. Chow, T. O. Xiao, R. C. Cammarata, Ed.: **1994**, *351*, 443.
[40] R. Bellissent, G. Galli, T. Hyeon, S. Magazu, D. Majolino, P. Migliardo, K. S. Suslick, *Phys. Scripta* **1995**, *T57*. 79.
[41] K. S. Suslick, T. Hyeon, M. Fang, *Chem. Mater.* **1996**, *8*, 2172.
[42] R. Bellissent, G. Galli, T. Hyeon, P. Migliardo, P. Parette, K. S. Suslick, *J. Noncryst. Solids* **1996**, *205*, 656.
[43] R. D. Rutledge, W. H. Morris, M. S. Wellons, Z. Gai, J. Shen, J. Bentley, J. E. Wittig, C. M. Lukehart, *J. Am. Chem. Soc.* **2006**, *128*, 14210.
[44] Y. Mizukoshi, K. Okitsu, Y. Maeda, T. A. Yamamoto, R. Oshima, Y. Nagata, *J. Phys. Chem. B* **1997**, *101*, 7033.
[45] Y. Mizukoshi, T. Fujimoto, Y. Nagata, R. Oshima, Y. Maeda, *J. Phys. Chem. B* **2000**, *104*, 6028.
[46] D. Radziuk, D. Shchukin, H. Mohwald, *J. Phys. Chem. C* **2008**, *112*, 2462.
[47] R. Basnayake, Z. Li, S. Katar, W. Zhou, H. Rivera, E. S. Smotkin, D. J. Casadonte, C. Korzeniewski, *Langmuir* **2006**, *22*, 10446.

© 2010 WILEY-VCH Verlag GmbH & Co. KGaA, Weinheim

[48] B. Gates, B. Mayers, A. Grossman, Y. Xia, *Adv. Mater.* **2002**, *14*, 1749.
[49] B. T. Mayers, K. Liu, D. Sunderland, Y. Xia, *Chem. Mater.* **2003**, *15*, 3852.
[50] Y. Zhu, H. Li, Y. Koltypin, Y. R. Hacohen, A. Gedanken, *Chem. Commun.* **2001**, 2616.
[51] R. V. Kumar, Y. Koltypin, X. N. Xu, Y. Yeshurun, A. Gedanken, I. Felner, *J. Appl. Phys.* **2001**, *89*, 6324.
[52] P. Jeevanandam, Y. Koltypin, A. Gedanken, *Nano Lett.* **2001**, *1*, 263.
[53] S. Avivi, Y. Mastai, G. Hodes, A. Gedanken, *J. Am. Chem. Soc.* **1999**, *121*, 4196.
[54] S. Avivi, Y. Mastai, A. Gedanken, *Chem. Mater.* **2000**, *12*, 1229.
[55] K. V. P. M. Shafi, I. Felner, Y. Mastai, A. Gedanken, *J. Phys. Chem. B* **1999**, *103*, 3358.
[56] J. C. Yu, J. Yu, W. Ho, L. Zhang, *Chem. Commun.* **2001**, 1942.
[57] D. Qian, J. Z. Jiang, P. L. Hansen, *Chem. Commun.* **2003**, 1078.
[58] S.-H. Jung, E. Oh, K.-H. Lee, Y. Yang, C. G. Park, W. Park, S.-H. Jeong, *Cryst. Growth Des.* **2008**, *8*, 265.
[59] H.-M. Xiong, D. G. Shchukin, H. Möhwald, Y. Xu, Y.-Y. Xia, *Angew. Chem. Int. Ed.* **2009**, *48*, 2727.
[60] D. Zhang, H. Fu, L. Shi, C. Pan, Q. Li, Y. Chu, W. Yu, *Inorg. Chem.* **2007**, *46*, 2446.
[61] C. V. C. Krishnan, J. Burger, C. Chu, B., *J. Phys. Chem. B* **2006**, *110*, 20182.
[62] C.-J. Mao, H.-C. Pan, X.-C. Wu, J.-J. Zhu, H.-Y. Chen, *J. Phys. Chem. B* **2006**, *110*, 14709.
[63] D. P. Dutta, V. Sudarsan, P. Srinivasu, A. Vinu, A. K. Tyagi, *J. Phys. Chem. C* **2008**, *112*, 6781.
[64] M. Sivakumar, T. Takami, H. Ikuta, A. Towata, K. Yasui, T. Tuziuti, T. Kozuka, D. Bhattacharya, Y. Iida, *J. Phys. Chem. B* **2006**, *110*, 15234.
[65] J. Geng, J. J. Zhu, H. Y. Chen, *Cryst. Growth Des.* **2006**, *6*, 321.
[66] J. Z. Geng, J.-J. Lu, D.-J. Chen, H.-Y., *Inorg. Chem.* **2006**, *45*, 8403.
[67] J. Geng, W. H. Hou, Y. N. Lv, J. J. Zhu, H. Y. Chen, *Inorg. Chem.* **2005**, *44*, 8503.
[68] D. P. Dutta, R. Ghildiyal, A. K. Tyagi, *J. Phys. Chem. C* **2009**, *113*, 16954.
[69] Y. Wang, X. Tang, L. Yin, W. Huang, Y. R. Hacohen, A. Gedanken, *Adv. Mater.* **2000**, *12*, 1183.
[70] L. Zhang, J. C. Yu, *Chem. Commun.* **2003**, 2078.
[71] J. C. Yu, L. Zhang, J. Yu, *Chem. Mater.* **2002**, *14*, 4647.
[72] J. C. Yu, L. Z. Zhang, J. Lin, *J. Colloid Interface Sci.* **2003**, *260*, 240.
[73] J. C. Yu, L. Zhang, Q. Li, K. W. Kwong, A. W. Xu, J. Lin, *Langmuir* **2003**, *19*, 7673.
[74] S.-H. Jung, E. Oh, K.-H. Lee, W. Park, S.-H. Jeong, *Adv. Mater.* **2007**, *19*, 749.
[75] J. Lai, K. V. P. M. Shafi, K. Loos, A. Ulman, Y. Lee, T. Vogt, C. Estournes, *J. Am. Chem. Soc.* **2003**, *125*, 11470.
[76] T. Prozorov, B. McCarty, Z. Cai, R. Prozorov, K. S. Suslick, *Appl. Phys. Lett.* **2004**, *85*, 3513.
[77] H.-l. Li, Y.-c. Zhu, S.-g. Chen, O. Palchik, J.-p. Xiong, Y. Koltypin, Y. Gofer, G.A., *J. Solid State Chem.* **2003**, *172*, 102.
[78] S. M. Zhou, Y. S. Feng, L. D. Zhang, *Mater. Lett.* **2003**, *57*, 2936.
[79] S. M. Zhou, Y. S. Feng, L. D. Zhang, *J. Mater. Res.* **2003**, *18*, 1188.
[80] M. M. Mdleleni, T. Hyeon, K. S. Suslick, *J. Am. Chem. Soc.* **1998**, *120*, 6189.
[81] I. Uzcanga, I. Bezverkhyy, P. Afanasiev, C. Scott, M. Vrinat, *Chem. Mater.* **2005**, *17*, 3575.
[82] H. Wang, J. J. Zhu, J. M. Zhu, H. Y. Chen, *J. Phys. Chem. B* **2002**, *106*, 3848.
[83] J. Zhu, Y. Koltypin, A. Gedanken, *Chem. Mater.* **2000**, *12*, 73.
[84] J. J. Zhu, H. Wang, S. Xu, H. Y. Chen, *Langmuir* **2002**, *18*, 3306.
[85] X. Qiu, C. Burda, R. Fu, L. Pu, H. Chen, J. Zhu, *J. Am. Chem. Soc.* **2004**, *126*, 16276.
[86] Y. Xie, X. Zheng, X. Jiang, J. Lu, L. Zhu, *Inorg. Chem.* **2002**, *41*, 387.
[87] B. Li, Y. Xie, J. Huang, Y. Liu, Y. Qian, *Chem. Mater.* **2000**, *12*, 2614.
[88] H. L. Li, Y. C. Zhu, O. Palchik, Y. Koltypin, A. Gedanken, V. Palchik, M. Slifkin, A. Weiss, *Inorg. Chem.* **2002**, *41*, 637.
[89] B. Pejova, I. Grozdanov, D. Nesheva, A. Petrova, *Chem. Mater.* **2008**, *20*, 2551.
[90] B. C. Gates, *in Catalytic Chemistry*, Wiley & Sons, New York **1992**, pp. 406.
[91] T. A. Pecoraro, R. R. Chianelli, *J. Catal.* **1981**, *67*, 430.
[92] M. J. Ledoux, O. Michaux, G. Agostini, P. Panisscd, *J. Catal.* **1986**, *102*, 275.
[93] J. J. Zhu, S. Xu, H. Wang, J. M. Zhu, H.-Y. Chen, *Adv. Mater.* **2003**, *15*, 156.
[94] J. Geng, B. Liu, L. Xu, F. N. Hu, J. J. Zhu, *Langmuir* **2007**, *23*, 10286.
[95] S. F. Wang, F. Gu, M. K. Lu, *Langmuir* **2006**, *22*, 398.
[96] H. Zhou, T. Fan, D. Zhang, Q. Guo, H. Ogawa, *Chem. Mater.* **2007**, *19*, 2144.
[97] M. J. Murcia, D. L. Shaw, H. Woodruff, C. A. Naumann, B. A. Young, E. C. Long, *Chem. Mater.* **2006**, *18*, 2219.
[98] T. Hyeon, M. Fang, K. S. Suslick, *J. Am. Chem. Soc.* **1996**, *118*, 5492.
[99] J. D. Oxley, M. M. Mdleleni, K. S. Suslick, *Catal. Today* **2004**, *88*, 139.
[100] K. S. Suslick, D. J. Casadonte, *J. Am. Chem. Soc.* **1987**, *109*, 3459.
[101] K. S. Suslick, S. J. Doktycz, *J. Am. Chem. Soc.* **1989**, *111*, 2342.
[102] K. S. Suslick, S. J. Doktycz, *Chem. Mater.* **1989**, *1*, 6.
[103] S. J. Doktycz, K. S. Suslick, *Science.* **1990**, *247*, 1067.
[104] T. Prozorov, R. Prozorov, K. S. Suslick, *J. Am. Chem. Soc.* **2004**, *126*, 13890.
[105] V. G. Pol, A. Gedanken, J. Calderon-Moreno, *Chem. Mater.* **2003**, *15*, 1111.
[106] V. G. Pol, M. Motiei, A. Gedanken, J. Calderon-Moreno, Y. Mastai, *Chem. Mater.* **2003**, *15*, 1378.
[107] V. G. Pol, H. Grisaru, A. Gedanken, *Langmuir* **2005**, *21*, 3635.
[108] A.-L. Morel, S. I. Nikitenko, K. Gionnet, A. Wattiaux, J. Lai-Kee-Him, C. Labrugere, B. Chevalier, G. Deleris, C. Petibois, A. Brisson, M. Simonoff, *ACS Nano.* **2008**, *2*, 847.
[109] K. V. P. M. Shafi, A. Ulman, X. Yan, N. L. Yang, M. Himmelhaus, M. Grunze, *Langmuir* **2001**, *17*, 1726.
[110] K. V. P. M. Shafi, A. Ulman, A. Dyal, X. Yan, N. L. Yang, C. Estournes, L. Fournes, A. Wattiaux, H. White, M. Rafailovich, *Chem. Mater.* **2002**, *14*, 1778.
[111] Q. Chen, C. Boothroyd, G. H. Tan, N. Sutanto, A. M. Soutar, Z. T. Zeng, *Langmuir* **2008**, *24*, 650.
[112] T. Gao, T. Wang, *Chem. Commun.* **2004**, 2558.
[113] T. Gao, Q. Li, T. Wang, *Chem. Mater.* **2005**, *17*, 887.
[114] J.-E. Park, M. Saikawa, M. Atobe, T. Fuchigami, *Chem. Commun.* **2006**, 2708.
[115] G. Dantsin, K. S. Suslick, *J. Am. Chem. Soc.* **2000**, *122*, 5214.
[116] J. E. Jones, M. C. Cheshire, D. J. Casadonte, C. C. Phifer, *Org. Lett.* **2004**, *6*, 1915.
[117] J. Walter, M. Nishioka, S. Hara, *Chem. Mater.* **2001**, *13*, 1828.
[118] N. A. Dhas, K. S. Suslick, *J. Am. Chem. Soc.* **2005**, *127*, 2368.
[119] J. H. Bang, K. S. Suslick, *J. Am. Chem. Soc.* **2007**, *129*, 2242.
[120] N. Du, H. Zhang, B. D. Chen, J. B. Wu, X. Y. Ma, Z. H. Liu, Y. Q. Zhang, D. R. Yang, X. H. Huang, J. P. Tu, *Adv. Mater.* **2007**, *19*, 4505.
[121] J. Wang, K. P. Loh, Y. L. Zhong, M. Lin, J. Ding, Y. L. Foo, *Chem. Mater.* **2007**, *19*, 2566.
[122] J. Yin, X. Qian, J. Yin, M. Shi, G. Zhou, *Mater. Lett.* **2003**, *57*, 3859.
[123] X. H. Sun, C. P. Li, N. B. Wong, C. S. Lee, S. T. Lee, B. K. Teo, *J. Am. Chem. Soc.* **2002**, *124*, 14856.
[124] C. P. Li, B. K. Teo, X. H. Sun, N. B. Wong, S. T. Lee, *Chem. Mater.* **2005**, *17*, 5780.
[125] S. H. Jeong, J. H. Ko, J. B. Park, W. Park, *J. Am. Chem. Soc.* **2004**, *126*, 15982.
[126] L. M. Viculis, J. J. Mack, R. B. Kaner, *Science.* **2003**, *299*, 1361.
[127] K. S. Suslick, M. W. Grinstaff, *J. Am. Chem. Soc.* **1990**, *112*, 7807.
[128] M. W. Grinstaff, K. S. Suslick, *Proc. Natl. Acad. Sci. U. S. A.* **1991**, *88*, 7708.
[129] K. J. Liu, M. W. Grinstaff, J. Jiang, K. S. Suslick, H. M. Swartz, W. Wang, *Biophys. J.* **1994**, *67*, 896.
[130] K. S. Suslick, M. W. Grinstaff, K. J. Kolbeck, M. Wong, *Ultrason. Sonochem.* **1994**, *1*, S65.
[131] A. G. Webb, M. Wong, K. J. Kolbeck, R. L. Magin, L. J. Wilmes, K. S. Suslick, *J. Magn. Reson. Imaging* **1996**, *6*, 675.

WILEY InterScience® DISCOVER SOMETHING GREAT
© 2010 WILEY-VCH Verlag GmbH & Co. KGaA, Weinheim

[132] J. J. Eckburg, J. C. Chato, K. J. Liu, M. W. Grinstaff, H. M. Swartz, K. S. Suslick, F. P. Auteri, *J. Biomech. Eng.* **1996**, *118*, 193.
[133] F. J.-J. Toublan, S. Boppart, K. S. Suslick, *J. Am. Chem. Soc.* **2006**, *128*, 3472.
[134] E. M. Dibbern, F. J.-J. Toublan, K. S. Suslick, *J. Am. Chem. Soc.* **2006**, *128*, 6540.
[135] S. Biggs, F. Grieser, *Macromolecules.* **1995**, *28*, 4877.
[136] M. Bradley, M. Ashokkumar, F. Grieser, *J. Am. Chem. Soc.* **2003**, *125*, 525.
[137] H. K. Kim, K. Matyjaszewski, *J. Am. Chem. Soc.* **1988**, *110*, 3321.
[138] T. T. Kodas, M. Hampden-Smith, *Aerosol Processing of Materials*, Wiley-VCH, New York **1999**.
[139] K. Okuyama, W. Lenggoro, *Chem. Eng. Sci.* **2003**, *58*, 537.
[140] G. L. Messing, S.-C. Zhang, G. V. Jayanthi, *J. Am. Ceram. Soc.* **1993**, *76*, 2707.
[141] R. W. Wood, A. L. Loomis, *Phil. Mag.* **1927**, *7*, 417.
[142] R. J. Lang, *J. Acoustical Soc.* **1962**, *34*, 6.
[143] I. W. Lenggoro, T. Hata, F. Iskandar, M. M. Lunden, O.K., *J. Mater. Res.* **2000**, *15*, 733.
[144] P. S. Patil, *Mater. Chem. Phys.* **1999**, *59*, 185.
[145] T. C. Pluym, Q. H. Powell, G.A.S., T. L. Ward, T. T. Kodas, L.-M. Wang, H. D. Glicksman, *J. Aerosol Sci.* **1993**, *24*, 383.
[146] T. C. Pluym, S. W. Lyons, Q. H. Powell, A. S. Gurav, T. T. Kodas, L.-M. Wang, H. D. Glicksman, *Mater. Res. Bull.* **1993**, *28*, 369.
[147] D. Majumdar, T. T. Kodas, H. D. Glicksman, *Adv. Mater.* **1996**, *8*, 1020.
[148] J. H. Kim, T. A. Germer, G. W. Mulholland, S. H. Ehrman, *Adv. Mater.* **2002**, *14*, 518.
[149] K. Nagashima, M. Wada, A. Kato, *J. Mater. Res.* **1990**, *5*, 2828.
[150] S. Gürmen, S. Stopić, B. Friedrich, *Mater. Res. Bull.* **2006**, *41*, 1882.
[151] T. C. Pluym, T. T. Kodas, L.-M. Wang, H. D. Glicksman, *J. Mater. Res.* **1995**, *10*, 1661.
[152] J. H. Kim, V. I. Babushok, T. A. Germer, G. W. Mulholland, S. H. Ehrman, *J. Mater. Res.* **2003**, *18*, 1614.
[153] S. R. C. Vivekchand, G. Gundiah, A. Govindaraj, C. N. R. Rao, *Adv. Mater.* **2004**, *16*, 1842.
[154] Y. C. Kang, H. S. Roh, S. B. Park, *Adv. Mater.* **2000**, *12*, 451.
[155] B. Xia, I. W. Lenggoro, K. Okuyama, *Chem. Mater.* **2002**, *14*, 4969.
[156] I. W. Lenggoro, Y. Itoh, K. Okuyama, T. O. Kim, *J. Mater. Res.* **2004**, *19*, 3534.
[157] I. W. Lenggoro, C. Panatarani, K. Okuyama, *Mater. Sci. Eng. B* **2004**, *113*, 60.
[158] K. Y. Jung, H. W. Lee, Y. C. Kang, S. B. Park, Y. S. Yang, *Chem. Mater.* **2005**, *17*, 2729.
[159] S.-H. Park, S. W. Oh, Y.-K. Sun, *J. Power Sources* **2005**, *146*, 622.
[160] Y. Huang, Z. Zheng, Z. Ai, L. Zhang, X. Fan, Z. Zou, *J. Phys. Chem. B* **2006**, *110*, 19323.
[161] C. R. Michel, E. R. López, H. R. Zea, *Mater. Res. Bull.* **2006**, *41*, 209.
[162] D. Jugović, N. Cvjetićanin, V. Kusigerski, M. Mitrić, M. Miljković, D. Makovec, D. Uskoković, *Mater. Res. Bull.* **2007**, *42*, 515.
[163] T.-H. Teng, M.-R. Yang, S.-h. Wu, Y.-P. Chiang, *Solid State Commun.* **2007**, *142*, 389.
[164] W.-N. Wang, W. Widiyastuti, I. W. Lenggoro, T. O. Kim, K. Okuyama, *J. Electrochem. Soc.* **2007**, *154*, J121.
[165] C.-L. Chang, C.-S. Hsu, B.-H. Hwang, *J. Power Sources* **2008**, *179*, 734.
[166] R. R. Chamberlin, J. S. Skarman, *J. Electrochem. Soc.* **1966**, *113*, 86.
[167] M. E. Davis, *Nature* **2002**, *417*, 813.
[168] G. J. d, A. Soler-Illia, C. Sanchez, B. Lebeau, J. Patarin, *Chem. Rev.* **2002**, *102*, 4093.
[169] S. W. Boettcher, J. Fan, C.-K. Tsung, Q. Shi, G. D. Stucky, *Acc. Chem. Res.* **2007**, *40*, 784.
[170] M. G. Kanatzidis, *Adv. Mater.* **2007**, *19*, 1165.
[171] C. J. Brinker, Y. Lu, A. Sellinger, H. Fan, *Adv. Mater.* **1999**, *11*, 579.
[172] Y. Lu, H. Fan, A. Stump, T. L. Ward, T. Rieker, C. J. Brinker, *Nature* **1999**, *398*, 223.
[173] X. Ji, Q. Hu, J. E. Hampsey, X. Qiu, L. Gao, J. He, Y. Lu, *Chem. Mater.* **2006**, *18*, 2265.
[174] H. Fan, F. Van Swol, Y. Lu, C. J. Brinker, *J. Non-Crystalline Solids* **2001**, *285*, 71.
[175] Y. Lu, B. F. McCaughey, D. Wang, J. E. Hampsey, N. Doke, Z. Yang, C. J. Brinker, *Adv. Mater.* **2003**, *15*, 1733.
[176] J. E. Hampsey, S. Arsenault, Q. Hu, Y. Lu, *Chem. Mater.* **2005**, *17*, 2475.
[177] X. Ji, J. E. Hampsey, Q. Hu, J. He, Z. Yang, Y. Lu, *Chem. Mater.* **2003**, *15*, 3656.
[178] J. H. Bang, S. H. Lim, E. Park, K. S. Suslick, *Langmuir* **2008**, *24*, 13168.
[179] L. Li, C.-K. Tsung, T. Ming, Z. Sun, W. Ni, Q. Shi, G. D. Stucky, J. Wang, *Adv. Funct. Mater.* **2008**, *18*, 2956.
[180] T. Zheng, J. Zhan, J. Pang, G. S. Tan, J. He, G. L. McPherson, Y. Lu, V. T. John, *Adv. Mater.* **2006**, *18*, 2735.
[181] C. Boissière, L. Nicole, C. Gervais, F. Babonneau, M. Antonietti, H. Amenitsch, C. Sanchez, D. Grosso, *Chem. Mater.* **2006**, *18*, 5238.
[182] L. Li, C.-K. Tsung, Z. Yang, G. D. Stucky, L. D. Sun, J. F. Wang, C. H. Yan, *Adv. Mater.* **2008**, *20*, 903.
[183] S. E. Skrabalak, K. S. Suslick, *J. Am. Chem. Soc.* **2005**, *127*, 9990.
[184] J. H. Bang, R. J. Helmich, K. S. Suslick, *Adv. Mater.* **2008**, *20*, 2599.
[185] W. H. Suh, A. R. Jang, Y.-H. Suh, K. S. Suslick, *Adv. Mater.* **2006**, *18*, 1832.
[186] J. E. Hampsey, Q. Hu, L. Rice, J. Pang, Z. Wu, Y. Lu, *Chem. Commun.* **2005**, 3606.
[187] Q. Hu, Y. Lu, G. P. Meisner, *J. Phys. Chem. C* **2008**, *112*, 1516.
[188] F. Iskandar, A. Mikrajuddin, K. Okuyama, *Nano Lett.* **2001**, *1*, 231.
[189] F. Iskandar, A. Mikrajuddin, K. Okuyama, *Nano Lett.* **2002**, *2*, 389.
[190] F. Iskandar, A. B. D. Nandiyanto, K. M. Yun, H.J.C.J., K. Okuyama, P. Biswas, *Adv. Mater.* **2007**, *19*, 1408.
[191] W. H. Suh, K. S. Suslick, *J. Am. Chem. Soc.* **2005**, *127*, 12007.
[192] Y. C. Kang, S. B. Park, *J. Aerosol Sci.* **1995**, *26*, 1131.
[193] I. W. Lenggoro, Y. Itoh, N. Iida, K. Okuyama, *Mater. Res. Bull.* **2003**, *38*, 1819.
[194] W.-N. Wang, I. W. Lenggoro, Y. Terashi, Y.-C. Wang, K. Okuyama, *J. Mater. Res.* **2005**, *20*, 2873.
[195] B. Xia, W. Lenggoro, K. Okuyama, *Adv. Mater.* **2001**, *13*, 1579.
[196] B. Xia, I. W. Lenggoro, K. Okuyama, *J. Mater. Chem.* **2001**, *11*, 2925.
[197] Y. Itoh, I. W. Lenggoro, K. Okuyama, L. Mädler, S. E. Pratsinis, *J. Nanopart. Res.* **2003**, *5*, 191.
[198] C. Panatarani, I. W. Lenggoro, K. Okuyama, *J. Nanopart. Res.* **2003**, *5*, 47.
[199] Y. Itoh, M. Abdullah, K. Okuyama, *J. Mater. Res.* **2004**, *19*, 1077.
[200] S. H. Kim, B. Y. H. Liu, M. R. Zachariah, *Chem. Mater.* **2002**, *14*, 2889.
[201] S. H. Kim, B. Y. H. Liu, M. R. Zachariah, *Langmuir* **2004**, *20*, 2523.
[202] X. Jiang, C. J. Brinker, *J. Am. Chem. Soc.* **2006**, *128*, 4512.
[203] T. Zheng, J. Pang, G. Tan, J. He, G. L. McPherson, Y. Lu, V. T. John, J. Zhan, *Langmuir* **2007**, *23*, 5143.
[204] S. E. Skrabalak, K. S. Suslick, *J. Am. Chem. Soc.* **2006**, *128*, 12642.
[205] S. E. Skrabalak, K. S. Suslick, *J. Phys. Chem. C* **2007**, *111*, 17807.
[206] J. H. Bang, K. Han, S. E. Skrabalak, H. Kim, K. S. Suslick, *J. Phys. Chem. C* **2007**, *111*, 10959.
[207] C. B. Murray, C. R. Kagan, M. G. Bawendi, *Annu. Rev. Mater. Sci.* **2000**, *30*, 545.
[208] K. Okuyama, I. W. Lenggoro, N. Tagami, S. Tamaki, N. Tohge, *J. Mater. Sci.* **1997**, *32*, 1229.
[209] Y. T. Didenko, K. S. Suslick, *J. Am. Chem. Soc.* **2005**, *127*, 12196.
[210] J. H. Bang, W. H. Suh, K. S. Suslick, *Chem. Mater.* **2008**, *20*, 4033.

© 2010 WILEY-VCH Verlag GmbH & Co. KGaA, Weinheim